Astron. Astrophys. 190, 289–319 (1988)

ASTRONOMY
AND
ASTROPHYSICS

CO $J=3-2$ and $J=2-1$ spectroscopy and mapping of ten high velocity molecular outflow sources

J.P. Phillips [1], G.J. White [1], R. Rainey [1], L.W. Avery [5], K.J. Richardson [1], M.J. Griffin [1], N.J. Cronin [2], T. Monteiro [3], and J. Hilton [4]

[1] Astrophysics Group., Department of Physics, Queen Mary College, Mile End Road, London, E1 4NS
[2] School of Physics, University of Bath
[3] School of Physics, University of Durham
[4] School of Mathematics, Goldsmiths College, London
[5] Herzberg Institute of Astrophysics, Ottawa, Canada

Received March 3, accepted May 31, 1987

Summary. We have mapped high velocity outflows associated with the sources K3-50, CRL 2591, W3, S88, NGC 2264, NGC 2024, S140, G35.2-0.74, NGC 1333 (HH 7-11), and NGC 1333 (IRAS 1) in the $J=2-1$ and $J=3-2$ transitions of CO. The line core and wing excitation properties are discussed in detail, and an approximate relation $dv/dr \simeq 2.5\ 10^{-4}\, n(H_2)^{3/2}\,\mathrm{km\,s^{-1}\,pc^{-1}}$ determined, whereby most of the nebulae appear to depart considerably from the régime of free-fall collapse, or thermal, turbulent, and rotational stability. Several sources in particular [cf. NGC 1333 (HH 7-11), S140, and NGC 2024] reveal a tendency to high outflow densities $n(H_2) \sim 10^4 \rightarrow 10^5\,\mathrm{cm^{-3}}$, and extremely low values of $X(CO)/dv/dr \sim 10^{-6} \rightarrow 10^{-8}$; a feature which may be indicative of large velocity gradients dv/dr, and shock refraction and compression at the edges of the outflow cavities. High and low density outflow environs are also frequently observed within the same source (cf. NGC 2024 and S140), and are perhaps indicative of varying degrees of shock deceleration near the outflow collimation zones. Four of the sources [S140, NGC 2024, NGC 1333 (HH 7-11), and NGC 1333 (IRAS 1)] show evidence for strongly attenuated $J=3-2$ radiation temperatures $T_R(J=3-2)$ compared with lower frequency transitions $J \rightarrow J-1$, a trend which in the case of NGC 1333 (IRAS 1) may be attributable to low kinetic temperatures T_k. For the remaining nebulae, however, it is found to be extremely difficult to simulate the observed line ratios through either homogeneous linear velocity field LVG models, source clumping, or self absorption. The possible contributions of infrared line pumping and non-linear velocity fields are also briefly considered, although it is concluded that non-LVG solutions may prove to be necessary.

Three of the molecular flows [S88, NGC 2264, and NGC 1333 (IRAS 1)] are revealed to be previously unrecognised bipolars, with S88 having a mechanical outflow energy of order $3\ 10^{45} \rightarrow 3\ 10^{46}$ erg, whilst the recently discovered bipolarity in NGC 2024 is confirmed through higher frequency mapping. The high velocities apparently present in this source, and which may account for the high degree of flow collimation, are adduced in favour of possible high levels of pre-shock H and He ionisation. This, in turn, is shown to have consequences for the excitation of the region as a whole, and the role of IRS 2 in contributing to the F1R luminosity, and the H II region ionising flux. A high proportion of the sources (S140, G35.2-0.74, and K3-50) are also found to have low and high velocity wings which appear co-spatial; a trend which may in part be attributed to high jet inclination $i \sim \pi/2$ to the line of sight, and/or low levels of flow collimation. An alternative mechanism in terms of co-spatial, high velocity, gravitationally bound turbulent elements is also briefly considered in the case of S140, and found to require an appreciable radial variation in density $n(H_2) \propto r^{\alpha}$, $\alpha > 1$. Finally, the sources S140, CRL 2591, and possibly G35.2-0.74 appear to possess significantly weaker counter jets, resulting in apparent monopolar configurations. The reasons for this are again not in all cases clear, although they may result from star formation near the edges of the placental clouds; one of the jets entering the primary cloud mass, and acquiring high post-shock column densities, CO opacities, and radiation temperatures $T_R(J \rightarrow J-1)$, the other exiting the cloud and encountering a very much lower density intercloud medium. Such a result agrees well with an LVG analysis for CRL 2591, in which the less confined jet would appear to possess the lower density, and a similar conformity is also noted for S88, in which the compact (and presumably more retarded) red flow is associated with the highest outflow densities.

Key words: bipolar outflows – CO $J=3-2$ and $J=2-1$ mapping

Send offprint requests to: J.P. Phillips

1. Introduction

High velocity molecular outflow sources have been the subject of considerable and intensive investigation over the last decade, and appear to represent an important phase of early stellar evolution, associated with both low and high mass pre-main-sequence stars (Lada, 1984, 1985). The outflow morphology appears in most cases to take a bipolar configuration, with evidence for high levels of flow collimation within $r \simeq 10^{16}$ cm of the driving source, and significantly lower levels of collimation at larger radial distances (Beiging et al., 1984). This, in turn, is presumably a consequence of more-or-less unconfined jet expansion outside of the collimating region, whereby the opening angle is determined by the ratio of the outflow to sonic velocities, or thermalisation of the jet leading to grossly increased thermal pressures. The nature of the collimating

zones is not well understood at present, although explanations in terms of radial cloud density gradients (Königl, 1982), and highly magnetised circumstellar disks (Draine, 1983; Puderitz and Norman, 1983) have been proposed.

An important question relating to these sources concerns their role in modulating GMC energetics and, in particular, the rate at which stars form (Franco and Cox, 1983; Lada and Gautier, 1982; Solomon et al., 1981). It has been known for some time that turbulent mass motion within GMCs is likely to dissipate over a fairly short time scale, comparable to the period of free-fall collapse, whence rapid star-formation and cloud dispersion would ensue (Field, 1978). In reality, however, it is clear that cloud turbulence must be continually renewed through mechanisms which are, as yet, ill defined. One possibility for maintaining cloud stability may involve high velocity molecular outflows (HMVOs) (Norman and Silk, 1978), and it is at least clear that the mechanical outflow energies of these sources (10^{43}–10^{47} erg) represent an appreciable contribution to the total cloud energy budgets. It is possible, therefore, that the star formation rate is determined by a rather delicate feed-back loop, whereby newly forming stars initiate HMVOs, increased cloud turbulence, and a reduction in subsequent collapse.

The investigation of such mechanisms, and the commonality of this phenomenon in early evolution, depends upon an understanding of the source statistics. Our understanding of the nature of HMVOs also depends upon a clear understanding of source morphology – what proportion of the sources are bipolars, for instance, and what is the characteristic mechanical energy outflow, outflow velocity, mass, and so forth. Several attempts have been made to address these problems, and of order of 10^2 HMVOs have been discovered to date. Relatively few of these have been investigated in any detail, however, although selective mapping suggests that a large proportion (perhaps ~75%) are probably bipolar.

In the following we present $J=3-2$ and $J=2-1$ mapping results for 10 HMVOs, aimed at investigating the morphology and kinematics of these zones. The observations for NGC 2024, S140, and W3 were obtained using the 3.6 metre Canada-France-Hawaii Telescope (CFHT) at Mauna Kea, Hawaii, whilst NGC 2264, S88, CRL 2591, K3-50, G35.2-0.74, NGC 1333 (IRAS 1) and NGC 1333 (HH 7-11) were observed using the 3.8 metre United Kingdom Infrared Telescope (UKIRT). In both cases, the results were taken with the Queesn Mary College Submillimetre Heterodyne receiver mounted at the Cassegrain focus, and a summary of central mapping reference positions is provided in Table 1.

Zenith transmission varied between the observing sessions, but was typically excellent, and of order 95% at 230 GHz and 85% at 345 GHz. Initial pointing and alignment were determined by peaking on the continuum emission from Jupiter, Saturn and Venus, and centring the optical image in the television guiding system. As result, absolute pointing is estimated to be of order 5″ or better in all cases. Calibration measures were obtained at approximately ten minute intervals using an ambient chopper vane to remove atmospheric attenuation and telescope losses. This technique gives a corrected antenna temperature scale, usually denoted by T_A^*, whilst the results presented in this paper are given in units of T_R^* (Kutner and Ulich, 1981), where $T_R^* = T_A^*/\eta_{\rm fss}$. The UKIRT values of the forward spillover $\eta_{\rm fss}$ were estimated as 0.85 for 345 GHz, and 0.88 at 230 GHz, whilst $\eta_{\rm fss}$ takes a 345 GHz value of 0.84 for the CFHT. The UKIRT and CFHT beamsizes were determined to be 55″ and 59″ at 345 GHz, and 83″ and 87″ at 230 GHz.

2. NGC 2024

NGC 2024 is a relatively close and compact area of the star formation (distance ~500 pc) connected with a more complex, widespread, and massive region of molecular and optical emission extending throughout Orion. In comparison with the nearby NGC 1976 and its environs, however, an area which includes molecular outflow sources, extensive blister zones, and multiple protostellar infrared sources, the Ori B region has been relatively poorly investigated to date. Radio maps at 15 and 23.4 GHz have been produced by Rodriguez and Chaisson (1978) and Krügel et al. (1982), for instance, and the region has also come under extensive recent scrutiny by Thronson et al. (1984), who have

Table 1. Observations of high velocity outflows

SOURCE	CENTRAL REFERENCE POSITION RA(1950) H :M : S	DEC(1950) D :M :S	J=2→1 CO	J=3→2 CO	OBSERVING FACILITY
K3-50	19:59:50.1	+33:24:19	-	✓	UKIRT
CRL 2591	20:27:35.9	+40:01:16	✓	✓	UKIRT
W3(IRAS)	02:21:53.2	+61:52:21	✓	✓	CFHT
S88	19:44:40	+25:05:30	✓	✓	UKIRT
NGC 2264	06:38:25	+09:32:25	-	✓	UKIRT
NGC 2024	05:39:14	-01:58:00	-	✓	CFHT
S140	22:17:41.9	+63:03:45	-	✓	CFHT
G35.2-0.74	18:55:41.1	+01:36:32	✓	✓	UKIRT
NGC 1333 (HH7-11)	03:25:58.2	+31:05:46	-	✓	UKIRT
NGC 1333 (IRAS1)	03:25:33.6	+31:03:14	✓	✓	UKIRT

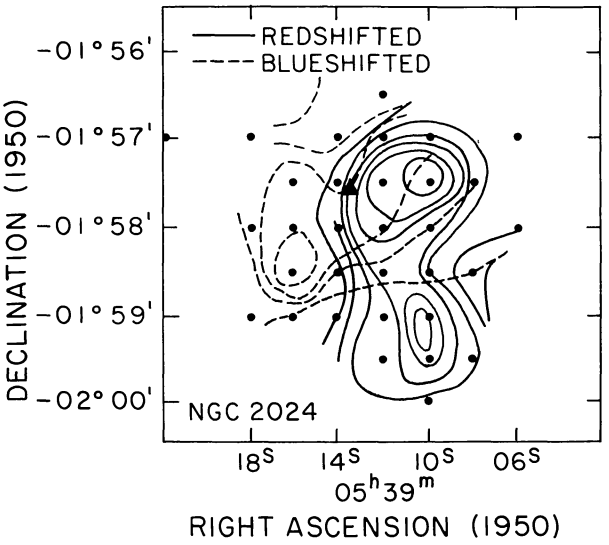

Fig. 1. Integrated $J=3-2$ CO red ($V_{LSR} \geqq 16\,km\,s^{-1}$) and blue ($V_{LSR} \leqq -7\,km\,s^{-1}$) wing emission in NGC 2024. Contours are set at increments of 3 K km s^{-1} (blue) and 4 K km s^{-1} (red) with the lowest red and blue contours taking the respective values 2 K km s^{-1}, and 4 K km s^{-1}

mapped the FIR continuum at λ40, 60, 100, and 160 μm. Molecular observations include CO $J=2-1$ mapping by Phillips et al. (1979), CO $J=3-2$ mapping by White et al. (1981), and most recently CS and HCN mapping and spectroscopy by Thronson et al. (1984) and Snell et al. (1984); results which reveal an extremely dense ($n_{H_2} \sim 10^6$ cm^{-3}) and possibly fragmented bar of neutral gas approximately co-spatial with the optical extinction. This in turn appears to partially obscure a region of optical emission with many of the characteristics of classical blister zones (cf. Icke et al., 1980), including displaced peaks of ionised hydrogen, near-, mid-, and far-infrared emission (cf. Frey et al., 1979). It is also likely that star-formation is occurring in dense regions of the nebula close to the ionised rim of the blister zone, with (in particular) evidence for H_2O maser emission close to the FIR peak (Genzel and Downes, 1977); an area which has also been investigated by Sanders and Willner (1985) in ^{12}CO ($J=1-0$, $J=2-1$) and ^{13}CO ($J=1-0$), and is the subject of the present discussion.

Sanders and Willner find that the maser is centred close to a highly collimated zone of CO emission, extending over some 6 arcminutes. Our present results in CO $J=3-2$, taken at broadly the same time, confirm the evidence for bipolarity over a more restricted area close to the maser position (Fig. 1). Whilst the southern red-shifted flow is fairly clearly established, at least for part of its length, a blueshifted wing peak is located to the east of the H_2O maser, and appears well separated from the area of redshifted emission. These general trends have subsequently been confirmed in recent higher resolution $J=1-0$ and $J=2-1$ observations (White et al., 1986).

Individual $J=3-2$ spectra for this source are also illustrated in Fig. 2, where the rapid variation of peak structure and line velocity width is notable. A further interesting feature is the presence of a single self-absorption trough in many of the core spectra – the line structure appearing rather less complex than at lower frequencies (cf. Sanders and Willner, 1983; Loren et al., 1981; Bally and Lada, 1983). Furthermore, and unlike the case in many other sources, the ratio between the self-absorption dip and peak temperatures appears not to increase greatly towards higher frequencies, and may indeed even decrease towards the centre. Where the reverse occurs, and the dip is more prominent at $J=3-2$, then this can usually be attributed to a lower density in the absorbing medium (as compared to the emission zone); a circumstance which might arise where, for instance, the sources have strong radial density and temperature gradients. On present evidence, therefore, one might conclude that core and absorbing layer densities are comparable, or at least that absorbing layer densities are not so low as to depopulate the $J=3$ CO rotational level. This, in reality, might very well prove the case, although we shall later meet complexities in the $J=3-2$ analysis which suggest that a degree of caution is advised.

2.1. Line core excitation conditions

The only published lower frequency CO data which permits direct comparison with the present results appears to be that of Loren et al. (1981), who present both $J=1-0$ and $J=2-1$ MWO spectra. Given the large size of this source at velocities corresponding to the line core components (cf. Phillips et al., 1979), the values of η_c for the MWO and UKIRT beams are large and comparable (~ 1.0), so that the relative intensities T_R^* illustrated in Fig. 3 are also comparable to the radiation temperatures T_R, and brightness temperatures T_B (providing dilution due to clumping is also negligible).

It is readily apparent that whilst temperatures for the CO $J=2-1$ results (corresponding to respective MWO beam-widths of 2'.4 and 1'.2) are closely comparable, the $J=3-2$ data is considerably weaker; a trend which appears also to apply for the blue-shifted emission at $V_{LSR} \sim 5\,km\,s^{-1}$. The behaviour of the core emission is of particular interest, since an homogeneous source (with unitary beam dilution at all three transitions) would be unlikely to yield the observed line ratios. To illustrate this, we have plotted the variation of radiation temperature $T_R(J=2-1)$ as a function of the maximum ratio ${}^M\Phi_{2/3} = T_R(J=2-1)/T_R(J=3-2)$ – a locus which is largely invariant with the assumed kinetic temperature T_k, excepting where T_k is very low (Fig. 4). Also located on this graph is the observed ratio $\Phi_{2/3}$ for NGC 2024, as well as values for several other of the sources to be considered here. In this, as for most of the proceeding analysis, we have employed a large velocity gradient (LVG) procedure (Goldreich and Kwan, 1974) to establish the statistical equilibrium population for $J \leqq 10$. Collision rate coefficients are taken from Green and Thaddeus (1976) and Green and Chapman (1978), and are appropriately weighted by a typical H_2/He abundance ratio.

As a result, it can be seen that the observed ratio at $T_R(J=2-1) \sim 30$ K is considerably larger than the maximum which could be achieved for a direct LVG analysis, a feature which appears also to apply for both HH7-11 and S140 (see later). Indeed, for any appreciable observed value of T_R we would expect Φ to be low and of order $\lesssim 1.5$.

It would appear, therefore, that the properties of this source must depart considerably from the uniform, homogeneous structure assumed above. Perhaps, for instance, the radius of the central core (or the size of individual clumps within the core) is a strongly varying function of transition frequency, yielding a dilution $W_{J=3-2}$ which is less than either $W_{J=2-1}$ or $W_{J=1-0}$. For this to occur, however, it is apparent that the optical depth $\tau(J=3-2)$ is required to be <1, and $\tau(J=2-1)$ and $\tau(J=1-0)$ greater than unity over most of the $J=1-0$ emission zone, a circumstance which we again find difficult to simulate using normal

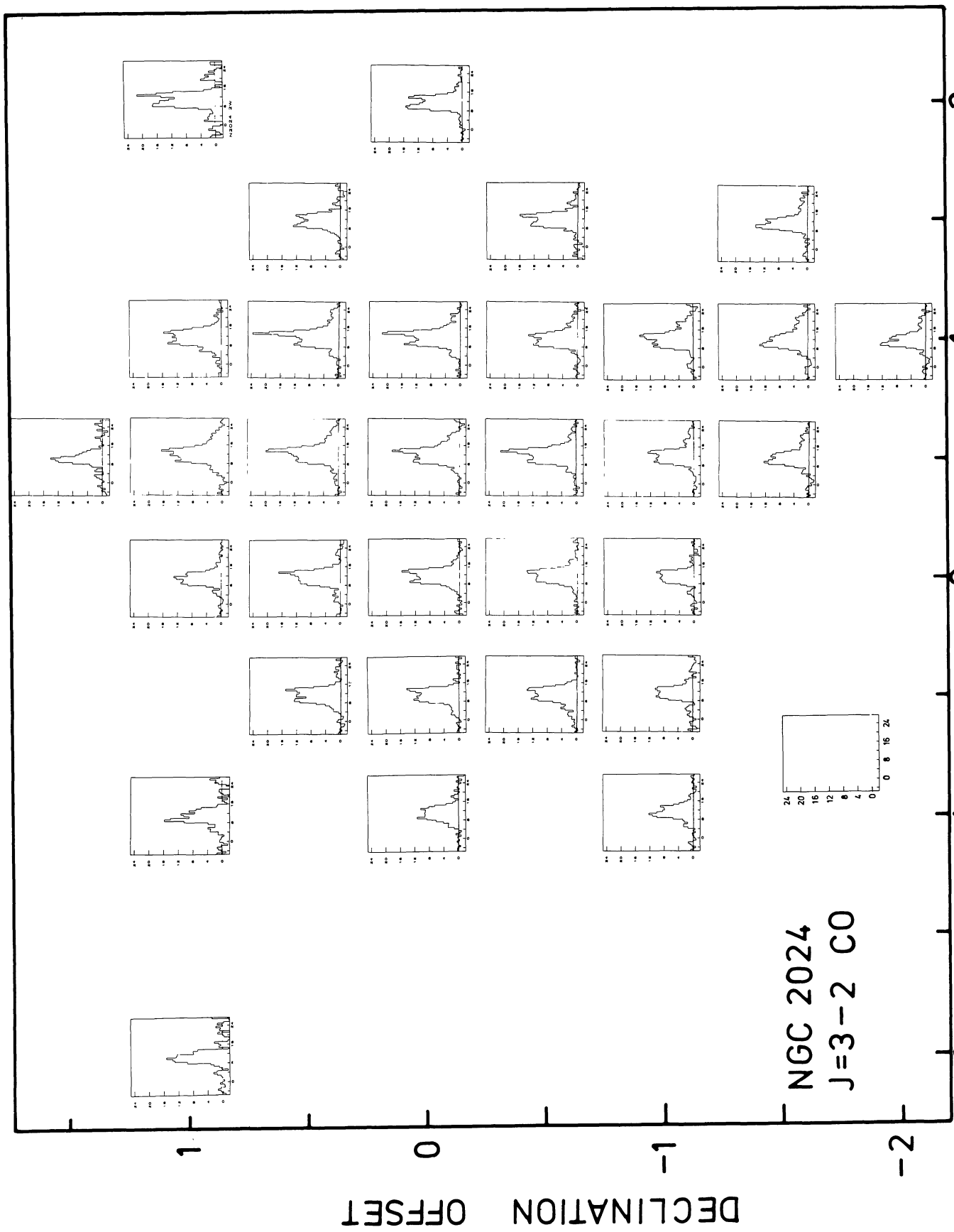

Fig. 2. $J=3-2$ CO spectra for NGC 2024. The [0, 0] position corresponds to the reference location in Table 1

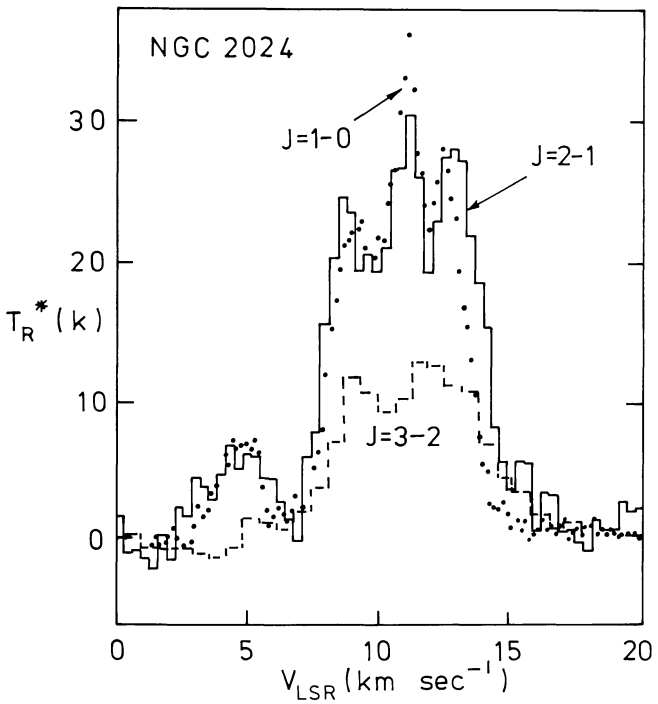

Fig. 3. Comparative $J=3-2$, $J=2-1$ and $J=1-0$ spectra for the [0, 0] position in NGC 2024. The $J=1-0$ and $J=2-1$ spectra are adapted from Loren et al. (1981). Note the severe attenuation of $J=3-2$ core and blue wing emission, although for the red wing it appears that $T_R(J=3-2) > T_R(J=1-0)$

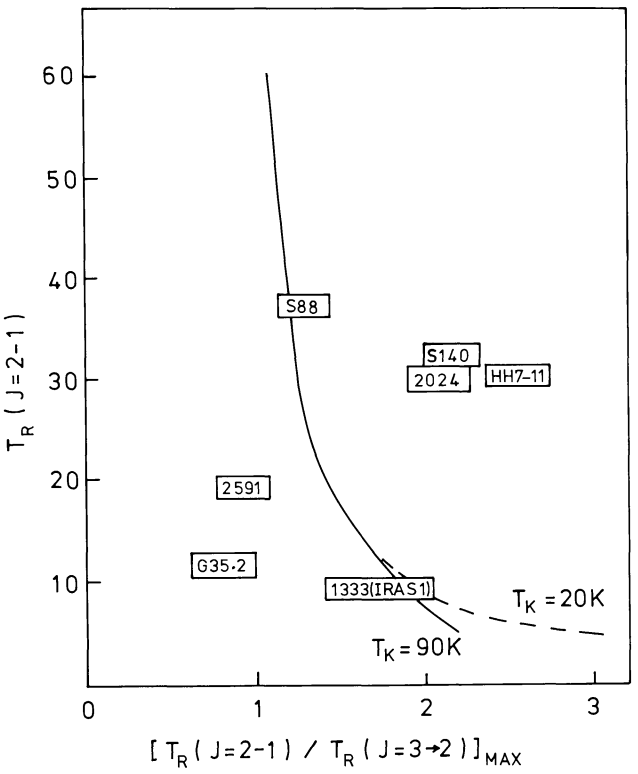

Fig. 4. Variation of the maximum value of $T_R(J=2-1)/T_R(J=3-2)$ as a function of $T_R(J=2-1)$ and T_K

LVG procedures. For the parametric ranges $20 < T_k < 100$ k, $-8 < \log(X(\mathrm{CO})/dv/dr) < -3$, and $2.8 < \log n(\mathrm{H_2}) < 5.3$, for instance, we find that τ_{3-2}/τ_{2-1} and τ_{3-2}/τ_{1-0} are both less than unity providing that $\log(X(\mathrm{CO})/dv/dr) \lesssim -5.5$ and $\log n(\mathrm{H_2}) \lesssim 3.0$. Under these circumstances, however, we also find that the $J=1-0$ optical depth takes a value $\ll 1$, and the levels of self-absorption would be all but negligible. It appears, therefore, that the concept of smaller, denser regions of the source dominating the higher frequency emission structure is not entirely practicable. Similar problems are also encountered if we suppose W to be <1, but invariant with transition $J \rightarrow J-1$. For this, more general case, the vertical axis in Fig. 4 corresponds to the function T_R/W, and for a given radiation temperature T_R it follows that the maximal value of $\Phi_{2/3}$ would be even smaller.

This leaves the possibility that the central line core as a whole is undergoing appreciable self-absorption; an hypothesis which would seem to be at least plausible, given the large emission spike at velocities $V_{\mathrm{LSR}} \sim 14\,\mathrm{km\,s^{-1}}$ – a feature suggestive of incomplete foreground absorption of a bright anterior source.

To investigate this situation more explicitly, therefore, we have adopted a two component model in which a dense, thermalised core has an invariant excitation temperature ${}^BT_e(J \rightarrow J-1)$, and brightness temperature ${}^BT_B(J-\Delta J-1)$. This is enveloped by a zone with density $n_c(\mathrm{H_2})$, kinetic temperature T_k, and optical depth $\tau_c(J \rightarrow J-1)$, whence observed core radiation temperatures are given by

$$T_{SA} = \left[\frac{2hBJ}{k}\right]\left[\frac{\exp(-\tau_c(J\rightarrow J-1))}{(\exp(2hBJ/k\,{}^BT_e)-1)} + \frac{1-\exp(-\tau_c(J\rightarrow J-1))}{(\exp(2hBJ/k\,{}^cT_e)-1)}\right],$$

where ${}^cT_e$ is the excitation temperature of the absorbing cloud, and other terms have their usual meanings.

We have explored a wide range of models in which ${}^BT_B > {}^cT_k$, and also ${}^BT_B$ is $<{}^cT_k$; typical examples are illustrated in Fig. 5. In Fig. 5a and b for instance we note that higher temperatures occur in the régime of low foreground absorption $\tau_c(\log X(\mathrm{CO})/dv/dr \lesssim -6)$, wherein $\Phi_{2/3}$ and $\Phi_{1/2}$ are also low, whilst higher values of Φ arise towards greater foreground optical depths $(\log X(\mathrm{CO})/dv/dr > -6)$, low line thermalisation $(\log n(\mathrm{H_2}) \lesssim 4)$, and lower antennae temperatures T_{SA}. As a result we find it extremely difficult to simulate the observed combinations of large $\Phi_{2/3}$, a modest $\Phi_{1/2}$, and high $T_{\mathrm{SA}}(J=1-0)$ – a situation which is barely alleviated by allowing for a more realistic variation in background excitation temperatures ${}^BT_e$. Similarly, where ${}^BT_B$ is $<{}^cT_k$ (corresponding, say, to the immersion of cool clumps within a warmer, interclump medium), then the deduced values of $\Phi_{2/3}$ are again no greater than would be deduced for the homogeneous model in Fig. 3.

Generally speaking, it would seem that although self-absorption is undoubtedly important over a wide range of values V_{LSR}, a simple LVG analysis is not readily able to simulate the observed trends. It is also clear, furthermore, that this problem of analysis is not confined to NGC 2024, but must also apply to the other sources in Fig. 4 having large values of $\Phi_{2/3}$. The problem is therefore widespread, and acts as a salutory reminder of the limits of such an analysis, and the caution which should be exercised in employing these techniques. A further, more extensive discussion of non-LVG procedures will be provided elsewhere, and other possible contributions are detailed in Sect. 12.

2.2. *Line wing excitation conditions*

The relative variation of line temperatures in the blue wing is very much as for the peak, although the absolute values of T_R are, of

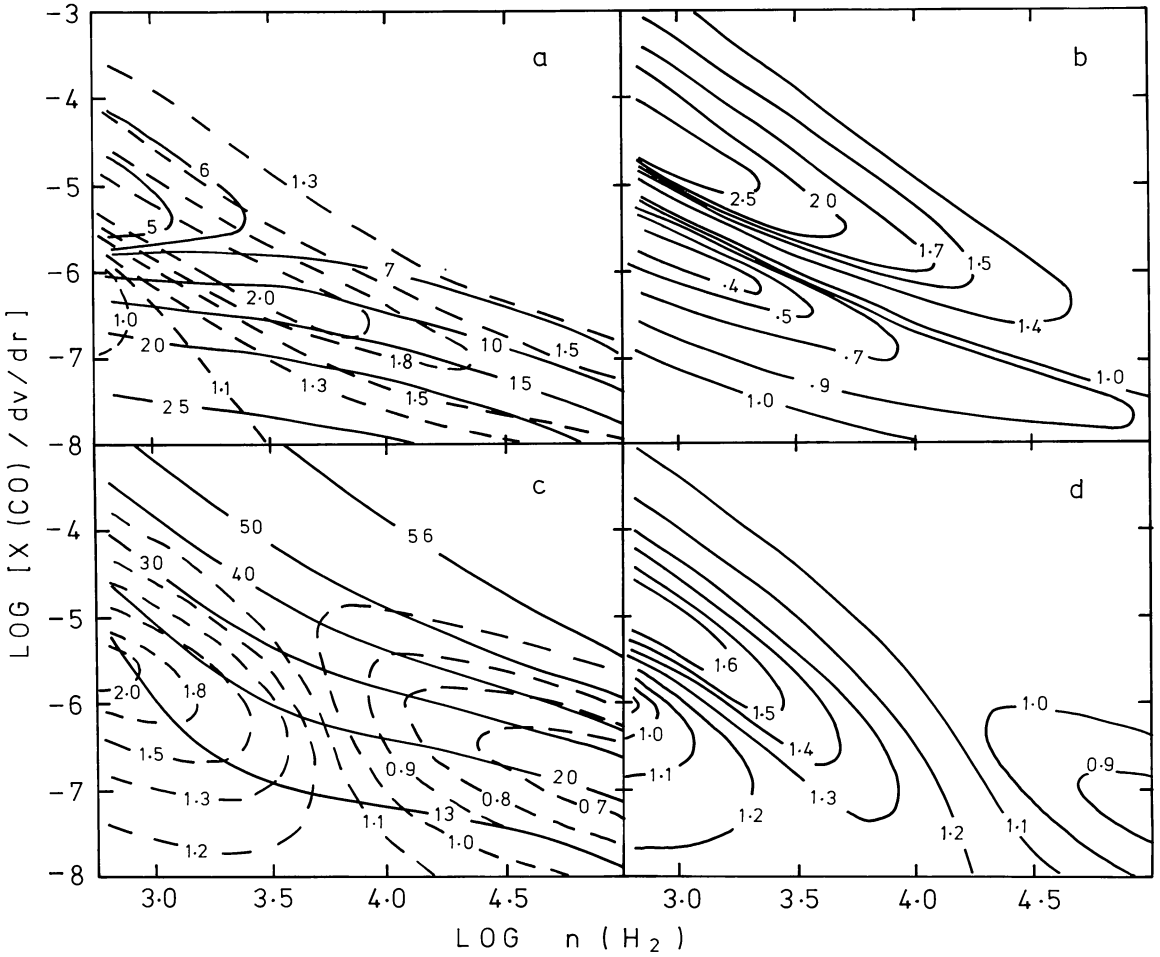

Fig. 5. LVG self-absorption modelling for ${}^{C}T_K = 10$ K, ${}^{B}T_e = 30$ K (panels a, b), and ${}^{C}T_K = 60$ K, ${}^{B}T_e = 15$ K (panels c, d). Panels (a) and (c) represent the variations of $T_{SA}(J=1-0)$ (———), and $\varphi_{1/2} = T_{SA}(J=1-0)/T_{SA}(J=2-1)$ (– – –). Panels (b) and (d) represent the variation $\varphi_{2/3} = T_{SA}(J=2-1)/T_{SA}(J=3-2)$

course, considerably smaller. Whether this relative core/wing temperature disparity is due to beam dilution effects, or reflects the conditions of excitation in the wing emission zone is uncertain; both effects will be considered below. There is evidence in other sources, however, that wing kinetic temperatures are likely to be appreciable, and we shall initially assume a value $T_k \sim 35$ k; similar to the presumed core excitation temperature. First of all, however, we note that irrespective of the absolute value of W, and presuming only that $W(J \rightarrow J-1)$ is invariant, then the observed ratio $T_R(1-0/T_R(2-1)$ at the velocity of peak wing emission implies $\log n(H_2) \lesssim 3.25$; and very similar constraints are also imposed given that $T_R(2-1)/T_R(3-2) \gtrsim 3$. This upper limit becomes, in turn, even smaller as the assumed value of T_k is increased, and it is clear that given the assumptions above, then the density must be small. If, more specifically, we now take $W \simeq 1$, then a best fit solution is achieved for $\log n(H_2) \simeq 3.1 \pm 0.2$ and $\log(X(CO)/dv/dr) \simeq -5.75 \pm 0.3$.

Where alternatively $W \ll 1$, however, then densities of order $\log n(H_2) \sim 4$ would be required as brightness temperatures approach $T_B = T_R/W \sim 25$ K. This, of course, is by no means implausible, and may be expected where instability and fragmentation of dense, neutral, post-shock zone occurs. A further requirement of such a solution, however, is that $W(2-1)/W(3-2)$ is >1, approaching a value ~ 3 where $\log n(H_2) \sim 4$, and this would be rather less explicable. Specifically, at such high densities we would anticipate a reasonably high level of collisional excitation to the $J=3$ rotational level, resulting in an optical depth $\tau(3-2)$ which is greater than $\tau(2-1)$. The $J=3-2$ and $J=2-1$ emission zones would, thereby, be expected to be comparable, and dilution $W(J=3-2)$ may even be greater than at $J=2-1$.

On these grounds alone, therefore, we are inclined to argue that W must indeed be large, and $n(H_2)$ concommitantly small; a quite different regime, in fact, to that pertaining in the red wing.

For velocities $V_{LSR} \gtrsim 14$ km s^{-1} we find, typically, that $T_R(3-2) \sim T_R(2-1)$, whence an LVG analysis would imply $\log n(H_2) \gtrsim 4.25$ for $\log(X/dv/dr) < -5.5$. Such high densities are also confirmed by the weakness of the $J=1-0$ transition, for which we find values $T_R(1-0)/T_R(2-1)$ ranging between ~ 0.2 and 0.5, and for all three transitions combined we obtain $\log(X/dv/dr) = -7.6 \pm 0.4$, and $\log n(H_2) = 4.4 \pm 0.3$ for $W=1$, $T_R = 35$ K and $V_{LSR} = 15$ km s^{-1}; values which alter to $\log(X/dv/dr) \simeq -7.0$ and $\log n(H_2) \simeq 3.75$ where $T_k = 90$ K.

At this point, however, a further note of caution should be entered. The apparent size of the wing zone in Fig. 1 is $\sim 2'$, and if these dimensions were also reflected at shorter wavelengths, then the corrected $J=1-0$ radiation temperature would be of order $T_R \sim 49k$, and $\Phi_{1/2} \sim 3.1$. Such parameters would not permit viable LVG solutions to be obtained for any plausible value of T_k –

and indeed, the minimum value of (lower frequency) source size to permit such a solution appears to be $D \sim 3.6'$; a dimension which would yield closely similar line excitation parameters to those determined above. Such a dimension would be inconsistent with the mapping of Sanders and Willner (1985), however, and we may be forced to conclude that a simple LVG analysis is again strictly inapplicable.

The spectral features described above are also prevalent in various other of the sources to be considered here, and we have for this reason taken particular care to outline the reservations, uncertainties, and options available in modelling such a region. Further such qualifications will also be noted in our modelling of other sources. There is also the possibility, however, that the energetic outflow from this source has a direct bearing upon our understanding of the source energetics, and the location and nature of the exciting star(s) for this region. We shall therefore concentrate on these questions in the remaining discussion.

2.3. *Excitation of NGC 2024*

A candidate bipolar central star has been observed in the near infrared by Sanders and Willner (1985), who find an NIR magnitude $L \sim 10.6$ mag, although there are no corresponding estimates of extinction. It is clear however from the FIR that the overall cloud optical depth must be large (cf. Thronson et al., 1984), and the substantial CO optical depth would also imply high levels of extinction for a simple LVG formalism. The central star intrinsic brightness may, therefore, be adequate to power the entire region. It would be difficult in these circumstances, however, to understand the location and distribution of H II emission, and it is more than likely that other stars are also responsible for the observed range of cloud properties.

The source of ionising and FIR emission in this region represents a longstanding and, so far, somewhat intractable problem. The source IRS 2, for instance, seems ideally placed to explain the distribution of ionised material and FIR emission. A careful consideration suggests that if a factor $\eta \sim 0.7$ of the radiant flux is allowed to escape unabsorbed by dust (e.g. the star resides in an open blister-like formation), then given $A_v = 12 \pm 3$ mag of foreground extinction (Thompson et al., 1981) a B 0.1 I (BO III) star having $M_k = -5.0$ (-4.7) mags would come very close to explaining the observed near infrared brightness of IRS 2, the total FIR luminosity of the region, and the maintenance of the observed H II region, for which $N_c \sim 10^{48}$ ionising photons s^{-1} are required (Krügel et al., 1982). Such a star would certainly be a little subluminous compared with other type I supergiants (or alternatively superluminous compared with the giants), but would adequately explain the full range of phenomena – except one. The problem resides with the effective temperature of such a star. Adapting the analysis of Black and Willner (1984), for instance, we may determine a value

$$T_{\rm eff} = \left[\frac{4.59\ 10^{11}}{(1-\eta)} \frac{F_{\rm TOT}}{F\lambda} \left(\frac{\lambda}{\mu\rm m}\right)^{-4}\right]^{1/3} \rm K,$$

where $F_{\rm TOT}$ is the (observed) integrated flux for the region, and F_λ is the stellar continuum flux at wavelength $\lambda (= 2.2\,\mu$m). For $1-\eta \simeq 0.3$, therefore, we determine an effective temperature $T_{\rm eff} = 30{,}000$ K; a value in accordance with the spectral types suggested above. Krügel et al. (1982), however, have noted the local presence of He^+ emission, and this would require an effective temperature of at least $T_{\rm eff} \simeq 32{,}000$ K (e.g. Cesarsky, 1977). If however we simply increase the presumed effective temperature to match this limit – and thereby dramatically increase the He ionising flux – then the total H ionising flux would become inordinately large, all other factors being equal.

One way out of the this problem, suggested by Thompson et al. (1981) and Black and Willner (1984), is to dispense with IRS 2 as the exciting star altogether, under which circumstance one or more faint and so far undetected O 9.5–9 ZAMS stars may fulfil a similar role. Some such suggestion would certainly appear plausible; although the K band brightness of these stars would fall short of the IRS 2 continuum by ~ 2 mag. Is there, however, another possible explanation?

The present results, and those of Sanders and Willner (1985), suggest that there may indeed be a solution to the He^+ problem which would again resurrect IRS 2 as a possible exciting star. The outflow velocity range of the bipolar source appears to be of order $2V_W \sim 60$ km s^{-1}, for instance, and it is clear that the wing velocity range remains large along the entire length of the outflow lobes (Sanders and Willner: unpublished data). Given that the outflow zone has an inclination to the line of sight i which is almost certainly low (cf. Sanders and Willner), it is probable that the flow velocity along the lobes is exceptionally large and of order $V_W/\sin i$. Such a result is also not inconsistent with the observed collimation of the lobes. Where for instance the ambient medium does not exert an appreciable confining pressure, then the angular width θ of the outflow lobes would be of order $\theta \simeq V_T/V_r \cos i$, where V_T is the sonic (transverse) gas velocity, and V_r is the radial outflow velocity. Applied therefore to NGC 2440 this would again suggest velocities which are large, and perhaps of order $\sim((V_T/\theta)^2 + V_W^2)^{1/2} \approx 10^2$ km s^{-1} (implying, in turn, $\sin i \approx 0.3$). Whilst the overall outflow characteristics are therefore ill-determined there is a prima-facie case for supposing shock velocities to be high.

Where the molecular outflow is accelerated by a stellar wind, then at least two principal shock zones are likely to emerge – one between the wind and shocked-wind material, which may constitute a hot expansive bubble within the molecular envelope, and the other involving the swept-up ambient material. Considering for the moment the ambient gas, it is already apparent from the CS results that local gas densities are high and, indeed, it is interesting to note that the regime of dense material follows quite closely the projected outflow zone. Whether there is a causal connection between the two distributions is difficult at present to determine. Shocks in such high density regimes have not been extensively considered in the literature, although where shock velocities are high, say $V_r > 40 \rightarrow 50$ km s^{-1}, then classical J-type shocks will be generated. Where, in turn, such velocities exceed $V_r \gtrsim 70$ km s^{-1}, then the shock parameters are relatively independant of the state of the ambient cloud – post-shock temperatures exceed 10^5 K, and the resultant UV radiation will completely pre-dissociate and pre-ionise the pre-shock gas (cf. Shull and McKee, 1979). Indeed, for $V_r > 80$ km s^{-1} the radiation field becomes hard enough to dissociate He, such that He is completely (singly) ionised for $V_r > 10^2$ km s^{-1}. Under such circumstances, it is clear that whilst the underlying blister zone in NGC 2440 may mask any H^+ emission, we might expect to observe enhanced He^+ emission in the vicinity of outflow lobes.

Plotting the He^+ distribution of Krügel et al. (1982) onto the molecular outflow pattern of Sanders and Willner, we find that this in fact is the case. The He^+ emission is concentrated about IRS 2, and in the projected spatial region occupied by the northerly outflow lobe. Such a result is, of course, no more than suggestive. It does however indicate that the exciting star(s) for the blister zone need not, necessarily, have a high temperature

$>32{,}000$ K, but may well be congruent with IRS 2, the observed centrally located NIR point source. We would also expect, on this evidence, to see similar He^+ emission at the base of the southerly outflow lobe, and (perhaps detectable) high excitation near-infrared line components.

3. S140

The H II region S140 is sharply bounded to the east by the dark clouds L1202/L1294, with which it appears to be directly interacting (cf. Blair et al., 1978). The interface between these two zones is defined by a bright ionisation front, leading to a maximum in Hα emission strength, a rapid fall-off in CO column density, and a rather elevated local H_2 density (Hayashi et al., 1985). There is little doubt, in short, that shocks are leading to localised compression of the neutral material, and may well be responsible for instigating a phase of recent star formation. Several such protostars appear to be located close to S140 IRS, a region which is associated with an H_2O maser (White and Little, 1975; Genzel and Downes, 1979) several infrared sources (Harvey et al., 1978), and strong CO, ^{13}CO, HCN, and H_2CO emission (Blair et al., 1978). The emission from CS appears also to peak at this source, and has an overall extent $\sim 4\,\mathrm{arcmin}^2$ which is less than that for CO (Hayashi et al., 1985; Snell et al., 1984).

As a result of these investigations, therefore, it appears likely that a denser, and more compact neutral zone is located within the more tenuous CO cloud, and is positioned close to (but some distance from) a compressive ionisation front. Blair et al. (1978) in their extensive consideration of cloud energetics, noted that linewidths about S140 IRS were quite large, extending over a range $18.7\,\mathrm{km\,s^{-1}}$ at the $T_A^* = 1$ K level. More recently, Bally and Lada (1983) and Margulis and Lada (1985) have noted that the wings extend to $\Delta V_{\mathrm{LSR}} \sim 42\,\mathrm{km\,s^{-1}}$ at the $T_R^* = 100$ mK level, and Snell et al. (1984) have argued that the outflow is bipolar.

3.1. Observations and line excitation

Our $J=3-2$ data takes the form of 16 spectra centred about S140 IRS, details of which are illustrated in Fig. 6. The variation of T_R^* (peak) is moderately rapid, declining by $\sim 30\%$ over a distance of 1 arcmin, whilst the full line width is also peaked upon the central source, and takes a maximum value $\sim 24\,\mathrm{km\,s^{-1}}$ at the $T_R^* = 1$ K level; very similar to the widths prevailing at lower frequencies (Fig. 7). The profile shapes also appear to vary quite rapidly with position, with the maximum blue-shifted emission centred close to the infrared object. Whilst superficial examination of the central spectra reveals a profile not dissimilar to those at $J=1-0$ and $J=2-1$ (cf. Blair et al., 1978), direct comparison yields several notable discrepancies. For this purpose, we have taken the $J=1-0$ NRAO spectrum from Margulis and Lada (1985), the $J=2-1$ MWO spectrum spectrum of Snell et al. (1984), and our own $J=3-2$ central CFHT profile, corresponding to the respective beam sizes 66″, 72″, and 59″; beam dilutions, in short, should be broadly comparable for all cases. The antennae temperatures have been converted to radiation temperatures by assuming a source size $\sim 2'$, and adopting source coupling factors $\eta_c = 0.64$ (NRAO), 0.84 (CFHT), and 0.51 (MWO).

The result, as can be seen in Fig. 8, is that despite small differences in profile – differences which may reflect the differing beam sizes employed, rather than any intrinsic spectral line variations – the peak temperatures and line shapes are closely similar at $J=1-0$ and $J=2-1$. This is not however the case at $J=3-2$. Over most of the core profile the $J=3-2$ line intensity is very much less than that at $J=2-1$ and $J=1-0$, although the ratio $T_R^*(J=3-2)/T_R^*(J=2-1)$ increases gradually towards the blue wing, and extremely rapidly towards higher velocities, where it takes a value close to unity. Over much of the line core, therefore, we find a situation which is closely reminiscent to that obtaining in NGC 2024. Given the large value of $T_R(J=2-1)$, it is probable that the observed value of $\Phi_{2/3} = T_R(J=2-1)/T_R(J=3-2) \simeq 2.1$ at $V_{\mathrm{LSR}} = -8\,\mathrm{km\,s^{-1}}$ would be inconsistent with a simple LVG analysis. Furthermore, it is apparent that this conclusion also applies over the relatively wide velocity regime $-4 < V_{\mathrm{LSR}} < -19\,\mathrm{km\,s^{-1}}$. Where self-absorption is present and $\tau(3-2) < 1$, it is clear that it must switch on extremely rapidly at $V_{\mathrm{LSR}} = -4\,\mathrm{km\,s^{-1}}$, and fall-off equally rapidly at $V_{\mathrm{LSR}} = -17\,\mathrm{km\,s^{-1}}$, in the meantime maintaining a more-or-less constant absorption optical depth. In reality, however, it is clear that neither optically thin nor thick self-absorption is likely to explain these results, at least within the framework of an LVG analysis, and for reasons discussed in Sect. 2 we can also dismiss factors such as variable source clumpiness.

As for NGC 2024, in short, it is apparent that the rapid attenuation of linestrength at 346 GHz is most likely to be explainable through non-LVG processes.

The red wing behaviour is also similar to that in NGC 2024, with $T_R(J=3-2) \sim T_R(J=2-1) > T_R(J=1-0)$, although in this case it is apparent that beam dilution effects can be discounted. The ratio $T_R(J=1-0)/T_R(J=2-1)$ achieves, in consequence, a maximum value ~ 0.5 at $V_{\mathrm{LSR}} = -2\,\mathrm{km\,s^{-1}}$, increasing to unity at larger velocities (although noise levels make these estimates increasingly unreliable for $V_{\mathrm{LSR}} > 0\,\mathrm{km\,s^{-1}}$). Taking $T_k \sim 35$ K, therefore, we find a best fit solution of $\log n(\mathrm{H_2}) \simeq 4.6 \pm 0.4$, $\log(X(\mathrm{CO})/dv/dr) \simeq -7.4 \pm 0.6$ at $V_{\mathrm{LSR}} = 2\,\mathrm{km\,s^{-1}}$.

The blue-wing analysis is a little more problematic, primarily because of the reduced S/N for $V_{\mathrm{LSR}} > -18\,\mathrm{km\,s^{-1}}$. Taking the intensities at this latter velocity as representative, however, we find $\log n(\mathrm{H_2}) = 3.5 \pm 0.2$, and $\log(X(\mathrm{CO})/dv/dr) \simeq -6.5 \pm 0.3$; that is, densities are still appreciable, but certainly less than appears to be the case in the red wing.

Finally, a comparison of the ^{13}CO $J=2-1$ spectrum of Margulis and Lada (1985) with the ^{12}CO results in figure 8 reveals a profile which is considerably narrower, peaks at $V_{\mathrm{LSR}} \simeq 8\,\mathrm{km\,s^{-1}}$, and declines to extremely low intensities in both line wings. Despite the high wing densities suggested above, therefore, it is likely that the maximum line optical depth is associated with the peak $J=1-0$ and $J=2-1$ line temperatures. The wing optical depths, in comparison, are almost certainly quite low, from which it follows that the core line-of-sight depth must be considerably greater than is the case in the wings. Alternatively, of course, we must presume a value of dv/dr (wing) which is substantial, and which remains substantial over a considerable depth of material; a physical régime which, whilst not necessarily inexplicable, would certainly be most unusual.

3.2. Emission zone structure

Whether the red and blue components of wing emission are part of a broad underlying emission component, upon which is superimposed the narrower (and more widely distributed) line emission at $V_{\mathrm{LSR}} \sim -8\,\mathrm{km\,s^{-1}}$, is not entirely clear. Snell et al. (1984) attribute the line wings to a bipolar outflow source, although the integrated wing emission strengths are greatly disparate both at $J=1-0$ and, as can be seen in Fig. 8, at $J=2-1$

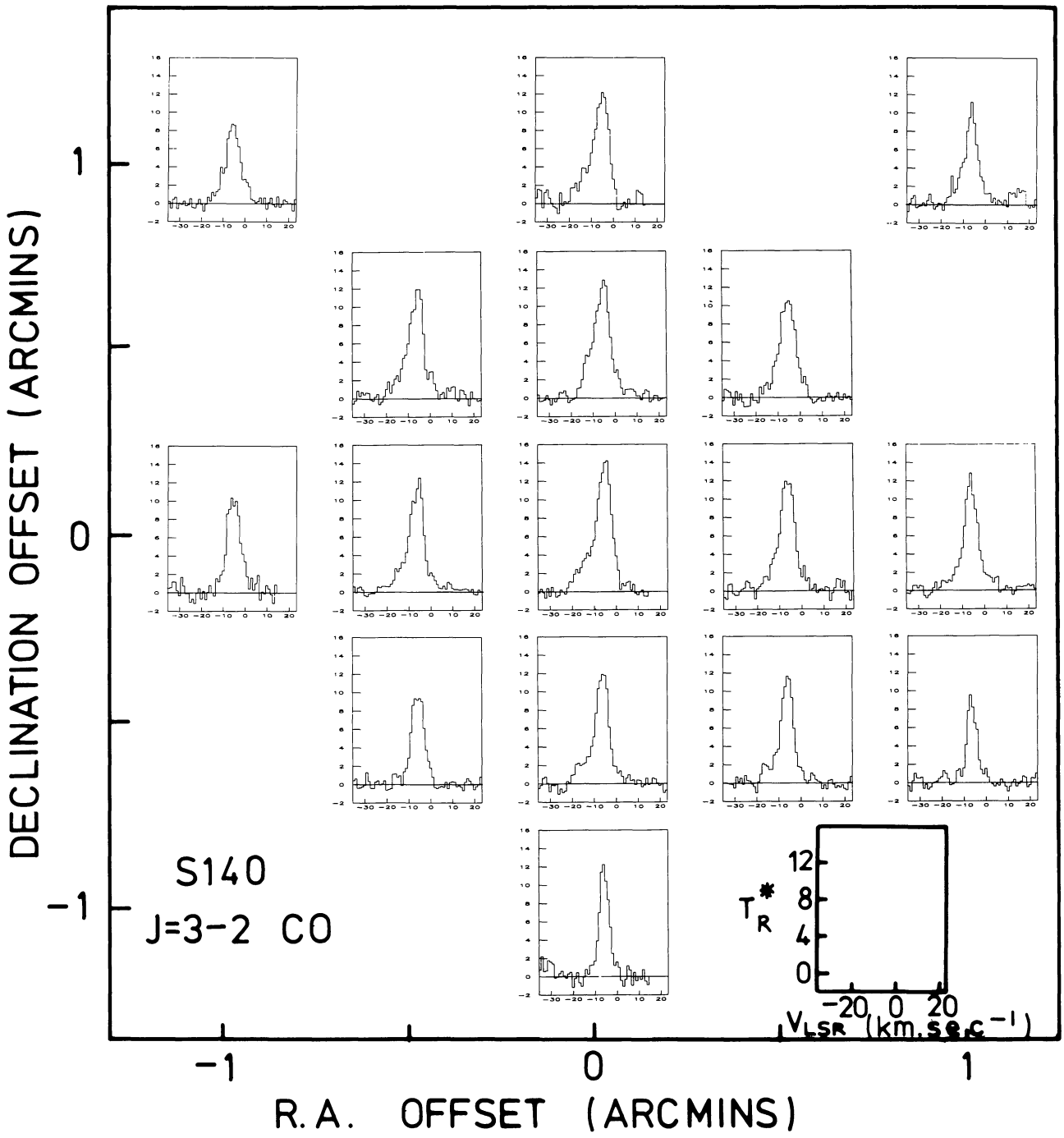

Fig. 6. $J=3-2$ CO spectra for S140. The [0,0] position corresponds to the reference location in Table 1

and $J=3-2$. A further problem with such an hypothesis concerns the proposed morphology of the outflow – the wings, as plotted by Snell et al. (1984), appear to extend away from S140 IRS *in the same direction*. Similarly, it is noteworthy that the wing emission structures are co-spatial with, and structurally similar to that of the CS cloud, with very little separation between the respective emission peaks. Our $J=3-2$ wing emission distributions are plotted in Fig. 7, and it is clear from this that the higher frequency results also replicate the trend at $J=1-0$; there is again very little differentiation between the wings at the $J=3-2$ resolution limit, although our mapping area is more compact.

Such a small separation of wing emission maxima might normally be ascribed to geometrical factors, and it is certainly true that many bipolar sources are almost certainly viewed along their outflow axes. This, however, can hardly apply here, given the relatively large and lop-sided extension of the wings. It might also be argued that the nearby ionisation front is in some way modifying flow properties (cf. Lada et al., 1984), although precisely how this is achieved in the present case remains uncertain.

A perhaps more plausible explanation, therefore, might be to regard the wings as extensions of the normal turbulent velocity field, generated in part by the mechanical energy input from

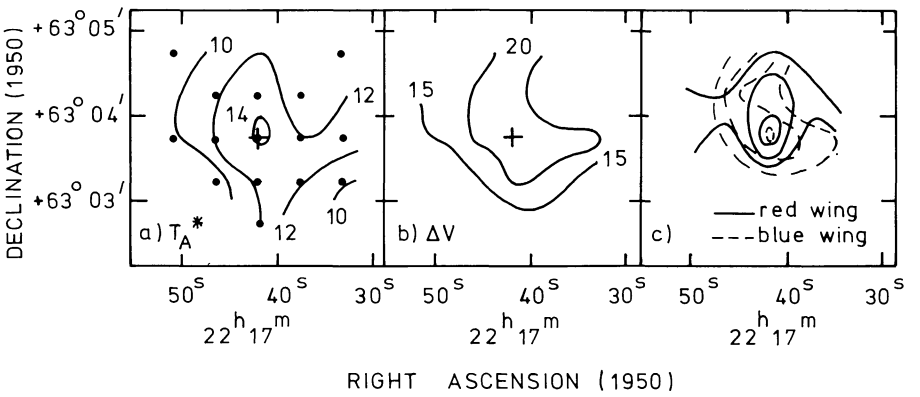

Fig. 7. The $J=3-2$ CO variation in T_R^* (peak), line width ΔV(km s^{-1}) at the $T_R^*=1$ K level, and integrated red ($-3 \leqq V_{LSR} \leqq 10$ km s^{-1}) and blue ($-30 \leqq V_{LSR} - 12$ km s^{-1}) wing distributions for S140. The integrated wing emission contours increment by 5 K km s^{-1}, with the lowest red contour set at 25 K km s^{-1}, and the lowest blue contour taking a value 15 K km s^{-1}

S140 IRS. If the wing features derive from higher density, high velocity clumps, bound by the CS mass condensation near S140 IR, then it would certainly be unsurprising to find similar CO wing, and CS line core/wing emission distributions. Can such an explanation be justified on dynamical grounds, however?

The answer, almost certainly, is in the affirmative. In this regard, we note that the FWHM of the ^{13}CO emission line is 3.8 km s^{-1}. If we assume that this intrinsic width represents the turbulent velocity field, and that virial equilibrium holds throughout this zone, then the overall cloud mass must be of order $M_c \sim 540\, M_\odot$ (we have assumed a cloud radius of 0.4 pc, and constant density. The mass estimate would decrease by a factor $\sim 3/5$ for an $r^{-\alpha}$, $\alpha = 2$ density fall-off). Such a value would in turn imply an H_2 column density $N(H_2) \sim 2.2\ 10^{17}\,\mathrm{cm}^{-2}$ which is consistent with deduced values of $N(^{13}\mathrm{CO})$ (Blair et al., 1978).

For the purposes of this discussion we equate the ^{13}CO $J=1-0$ FWHM with the root mean square turbulent velocity $(\langle V_T^2 \rangle)^{1/2}$, which is in turn taken to equal $(\langle$cloud kinetic energy$\rangle / M_c)^{0.5}$. Turbulent elements responsible for the wings, however, would be constrained to a velocity

$$V_0^2 \simeq \langle V_T^2 \rangle \frac{2}{(2-\alpha)} \frac{(5-2\alpha)}{(3-\alpha)} \qquad \alpha < 2$$

providing that they are gravitationally confined within the observed cloud boundaries. For $\alpha \sim 1.9$, therefore, we would find a value $(V_0^2/V_T^2\rangle)^{1/2} \sim 4.7$ which is little different from the observed ratio for $\Delta V_W / V_{\mathrm{FWHM}}$ (where ΔV_W is the full range of wing velocities) For $\alpha = 0$, on the other hand, it is clear that the maximum turbulent velocity would exceed $(\langle V_T^2 \rangle)^{1/2}$ by a factor of only 1.3, which would not be adequate to explain the observed velocity trends. Given, therefore, that the turbulent velocity spectrum may be complex, and perhaps part-modulated by local star formation, it appears that gravitationally confined turbulent elements may be capable of explaining the observed velocities in this source.

This is not, of course, to entirely rule out the possibility of jet activity, and the observed configuration is also consistent with a monopolar "flow"; although whether the counter-jet is absent, or simply so weak as to be unobserved, will require further measurements at a higher signal-to-noise. For the present, however, it would appear that the main (observed) jet is entering the primary H I mass, whilst the counter-jet is required to extend directly towards the H II region; a régime of notably low H I column densities. Under these circumstances, the counter-jet might be expected to encounter (and interact with) a relatively small amount of neutral material, and CO brightness temperatures would be correspondingly reduced; a configuration which is

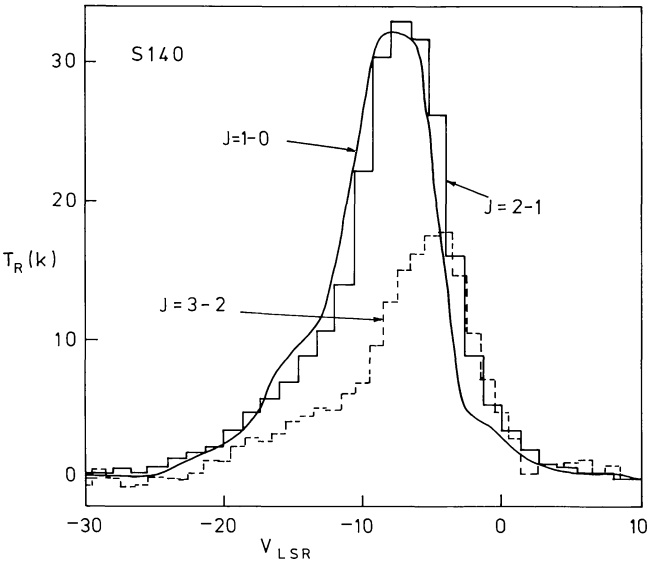

Fig. 8. Comparative $J=3-2$, $J=2-1$, and $J=1-0$ CO spectra of S140 at the [0,0] reference positin (Table 1). The $J=1-0$ spectrum is adapted from Margulis and Lada (1985), and the $J=2-1$ spectrum is taken from Snell et al. (1984)

highly reminiscent to that proposed for CRL 2591 (see later), a source in which a counter jet *has* been detected, but for which the CO $J=1-0$ lines are extremely weak (Sect. 5). Higher sensitivity observations of the counter jet location would clearly be of some considerable interest, although the less confined expansion régime resulting from the lower, intercloud densities may presumably result in a very much larger jet area than is at present observed.

Under these circumstances, therefore, the presence of co-spatial red *and* blue line wings can probably be taken to imply a jet inclination angle $i \lesssim \sin^{-1}(\theta/2)$, where θ is the jet opening angle. Both velocity wings would then arise not, primarily, from the radial flow of jet material, as from transverse expansion of the jet along the line-of-sight. It is clear, in consequence, that for both red and blue wings to be observed requires that i is small, and/or θ is large, leading (as in the present case) to poor outflow collimation.

4. K3-50

The K 3-50 nebula is located in a region of high extinction, and H II regions on a variety of size scales, and although classified as a

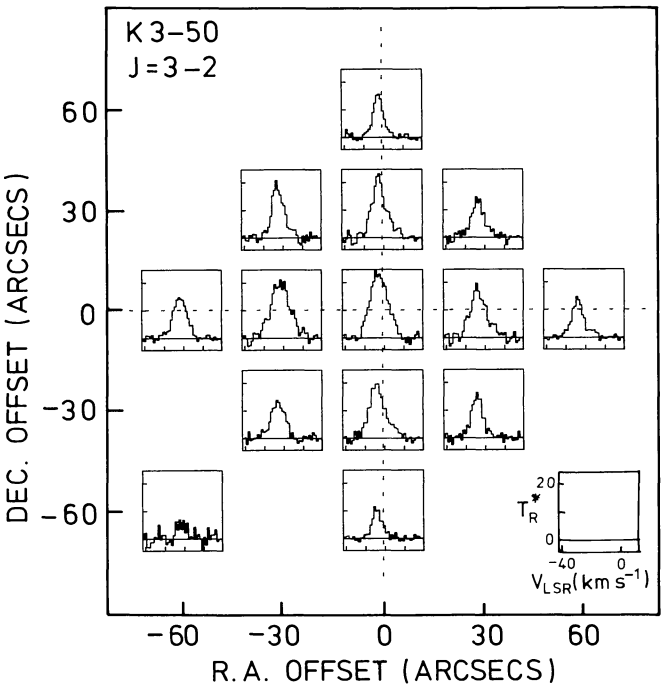

Fig. 9. CO $J=3-2$ spectra for K3-50. The [0,0] position corresponds to the reference location in Table 1

planetary nebula by Perek and Kohoutek (1967) is almost certainly associated with pre-main-sequence activity (Thronson and Harper, 1979). The ionised zone most directly associated with the optical nebulosity, designated K3-50A by Colley and Scott (1977), appears to be a highly compact shell structure with a diameter 2″ (Colley and Scott, 1977; Turner and Matthews, 1984), coincident with a strong 10 μm infrared peak (Wynn-Williams et al., 1977), and located ~2″ north-west of the visual nebula. Far infra-red mapping shows the source to be unresolved at $\lambda \sim 57$ μm, (30″ beam; Thronson and Harper, 1979) and $\lambda \sim 1$ mm (1′ beam; Wynn Williams et al., 1979), although photometry at $\lambda \sim 34$ μm (Wynn-Williams et al., 1977) suggests an emission zone which is larger than the H II region. At near infrared wavelengths, on the other hand, the source size becomes less than that of the H II shell region, and the emission peaks between 0.5 μm and 10 μm appear spatially displaced (Wynn Williams et al., 1977). The near-infrared colour temperature of the source is similarly found to take a value ~175 K (Wynn Williams et al., 1977), compared with a longer wave value of ~70 K found by Thronson and Harper (1979). This, together with other evidence discussed by Wynn Williams et al. (1977), suggests that the source is partially enveloped by a substantial dust cloud, the extinction through which is a strongly varying function of position. Little radio emission is associated with the optical nebulosity, and Wynn Williams et al. argue that this may represent a reflection nebulosity: the visibly section of a highly extincted, incipient blister zone which is presumably being observed from the side.

We have taken 14 CO $J=3-2$ spectra centred on the infrared source, and these are presented in Fig. 9. The peak value of T_R^* is 23 K at $V_{LSR} = -24$ km s^{-1}, similar to the central H_2CO velocity noted by Forster et al. (1982). At the IR position the half-power linewidth is ~12 km s^{-1}, a value which appears to decline to $\Delta V \sim 6$ km s^{-1} over a distance of 1 arcmin. The integral line flux is illustrated in Fig. 10a, together with the full width of the line to 1 K level (Fig. 10b), and it is clear that both of these parameters decline monotonically from the source reference location (Table 1). The full width $\Delta V_{LSR} \sim 20$ km s^{-1} of the spectral profiles suggests, in particular, that the central core source is a focus of considerable kinematic activity, and this (together with the asymmetric profiles) indicates a highly disturbed region. However, whilst the higher velocity components show evidence for rapid variability over small projected spatial distances, the evidence for bipolarity is at best marginal. This is also confirmed in Fig. 10d, where we have plotted both blue ($-34 < V_{LSR} < -30$ km s^{-1}) and red ($-11 < V_{LSR} < -18$ km s^{-1}) wing emission distributions. The integrated wing emission is seen to fall quite rapidly from the centre, and the broad distributions are very approximately co-spatial. The wing emission maxima are, however, clearly displaced, and this may indicate some tendency towards bipolarity. Further, more extensive (and preferably higher resolution) observations would clearly help clarify these trends.

5. CRL 2591

This interesting far-infrared source is located near an H_2O maser, and several compact sources of radio continuum emission (cf. Simon et al., 1981). Torrelles et al. (1983) and Bally and Lada (1983) have noted that molecular flow velocities are considerable in the vicinity of this source, and Torrelles et al were further able to show that the very much stronger blue-shifted wing emission occupies a region ~10 arcmin^2. Subsequently, Lada et al. (1984) obtained high signal to noise $J=1-0$ CO data which confirmed the high blue-shifted velocities, and revealed the presence of an extensive but considerably weaker red-shifted component. The

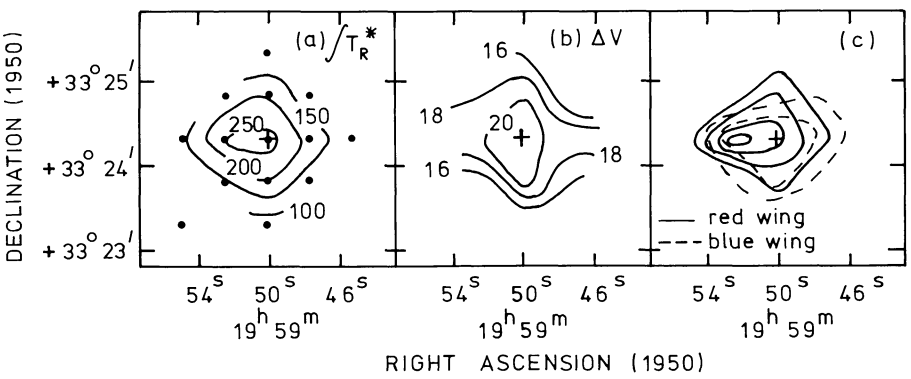

Fig. 10. $J=3-2$ CO variation in $T_R^* dv$, ΔV (km s^{-1}) at the $T_R^* = 1$ K level, and the red ($-18 \leqq V_{LSR} \leqq -11$ km s^{-1}) and blue ($-34 \leqq V_{LSR} \leqq -30$ km s^{-1}) wing emission distributions for K3-50. The integrated red-wing contours are set at 20, 30, 40, and 50 K km s^{-1}, whilst the corresponding blue wing contours are at 10 and 15 K km s^{-1}

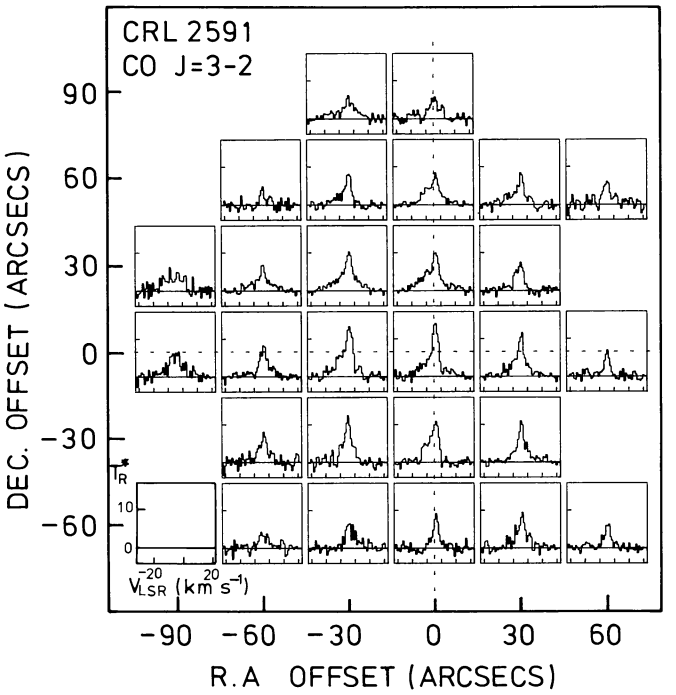

Fig. 11. CO $J=3-2$ spectra of CRL 2591. The [0,0] position corresponds to the reference location in Table 1

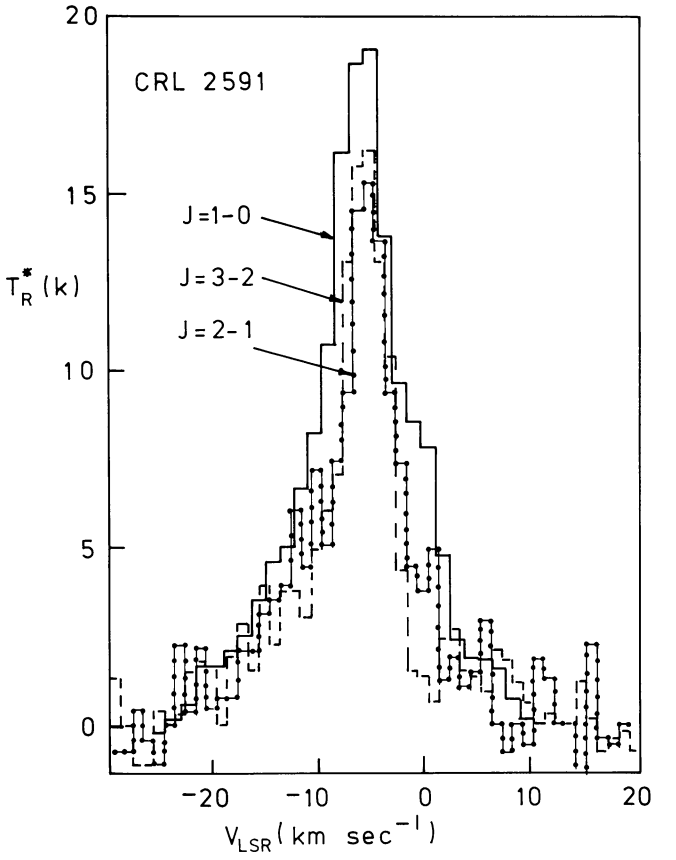

Fig. 12. Comparative $J=1-0$, $J=2-1$ and $J=3-2$ CO spectra for the [0,0] position in CRL 2591. The $J=1-0$ spectrum is derived from Torrelles et al. (1983)

reason for this exceptional disparity in wing strengths – a feature shown to this extent by only one other source, S140 – is not at all clear, although it is proposed by Lada et al. that the blue-shifted component is driving into a denser region of molecular cloud, leading to considerably larger masses of swept-up material. There is little evidence for radio emission at the central infrared source (Simon et al., 1981), a feature which presumably implies a driving star which is strongly pre-main-sequence. If this is true, however, then it is unlikely also to be responsible for the spatially displaced elements of local radio continuum emission, as proposed by Lada et al. (1984) – the O7.5 ZAMS star required to create the H II region southwest of the IR source would also be expected to generate at least some radio continuum at the central source itself.

We have taken spectra at 27 points about the central infrared source in $J=3-2$ CO, and these are detailed in Fig. 11. The strong blue-wing is clearly present at locations, primarily, north and west of the central source, in agreement with the mapping of Lada et al. (1984) and Torrelles et al. (1983). These trends are also present in our more limited mapping at $J=2-1$, the central spectrum of which is illustrated in Fig. 12. Few comparable $J=1-0$ spectra are available in the published literature, although Torrelles et al. (1983) and Bally and Lada (1983) illustrate spectra taken at the core. These, in turn, appear to show slight disparities, and there is little evidence in the spectrum of Torrelles et al. for the $+5\,\mathrm{km\,s^{-1}}$ component illustrated by Bally and Lada (1983), and discussed at some length by Lada et al. (1984). Such a component also appears to be largely absent from the present spectra, although our signal to noise is significantly poorer. Also weak in the present results, although not entirely absent, is evidence for any appreciable red-shifted component of emission. This is not entirely surprising, given again the lower S/N of our spectra, although we will also note further possible reasons for this disparity later this section.

A direct comparison of the Torrelles et al. core spectrum with our $J=2-1$ and $J=3-2$ data is provided in Fig. 12. For this case, we have converted antennae temperatures T_R^* and T_A^* into radiation temperatures T_R by assuming that wing and core line components emanate from broadly the same regions of sky (diameter $\sim 2'$, Fig. 13; see also Lada et al., 1984). More generally, of course, direct comparisons of this nature are fraught with problems, since wing and core line components have, almost invariably, differing spatial distributions. This would normally require differing beam coupling terms to be determined for each point in the spectrum, together with a detailed understanding of the wavelength variability in source structure. Needless to say, however, such an operation is rarely (if ever) essayed, and the resulting comparisons (particularly between spectra acquired with differing telescopes) may be quite misleading.

In the present case, however, it seems that our assumptions are not exceptionally gross, and the red and blue wing distributions are similar to that of the central line core. The result, as can be seen, is that peak line temperatures are reasonably consistent, implying excitation temperatures 22.3 K ($J=3-2$), 20.5 K ($J=2-1$), and 22.5 K ($J=1-0$). It appears, furthermore, that the strong blue-wing emission has comparable strength at all these frequencies.

This is not however the case for the red-shifted emission, which appears to decline precipitously and systematically with higher J transition. As a result, the $J=3-2$ CO lines appear significantly steeper to the redward side than is the case for lower frequency transitions. Such a trend is also, presumably, responsible for the steepsided spectra we observe to the south of CRL 2591.

Whilst a detailed analysis is somewhat compromised by the absence of comparable ^{13}CO data, several general comments may

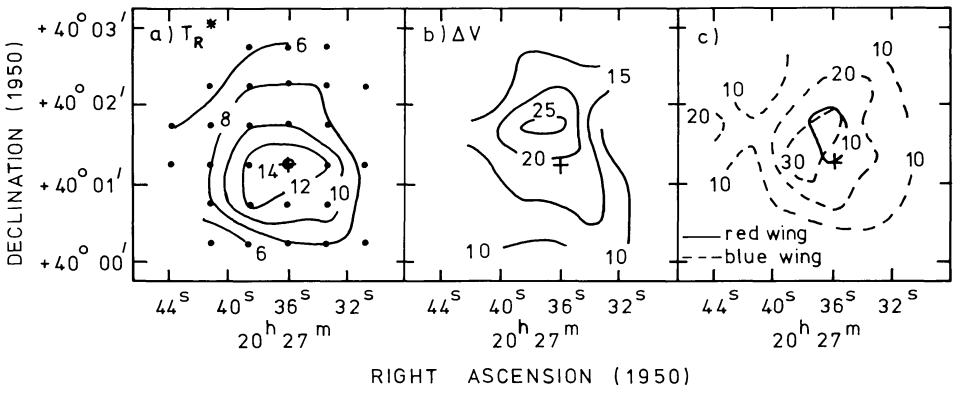

Fig. 13. Variation of T_R^* (peak), line width ΔV (km s^{-1}) at the $T_R^* = 1$ K level, and the integrated blue ($-22 \leqq V_{LSR} \leqq 10$ km s^{-1}) and red ($4 \leqq V_{LSR} \leqq 15$ km s^{-1}) wing emission distributions in CRL 2591

nevertheless be stated. In the first place, for instance, it is clear that such large $J=3-2/J=2-1$, $J=2-1/J=1-0$ ratios as are observed in the blue wings require densities $\log n(H_2) > 3.5\,\mathrm{cm}^{-3}$ for $\log X(CO)/dv/dr < 10^{-4}$; densities, in short, which are generally large. If the velocity gradients take a value $dv/dr \gg 1\,\mathrm{km\,s^{-1}\,pc^{-1}}$, on the other hand, then the ratio $T_R(3-2)/T_R(2-1)$ enables even tighter constraints on density, implying $X(CO)/dv/dr \geqq 2\,10^3\,n(H_2)^{-2.3}$; an expression which would yield $n(H_2) > 10^4\,\mathrm{cm}^{-3}$ for $\log(X(CO)/dv/dr < -5.6$, where we have assumed a kinetic temperature $T_k \sim T_{ex}(1-0) \sim 25$ K.

The blue wing, in short, appears likely to emanate from gas which has a reasonably high density, and this would also be consistent with the Lada et al. (1984) interpretation of flow morphology. The red wing, on the other hand, would require densities $\log(n(H_2)) \sim 2.8 \pm 0.3$, and values $\log(X(CO)/dv/dr) \sim -4.9 \pm 0.6$ to explain the precipitous decline in emission strength with increasing transition frequency. This, again, would not be inconsistent with the Lada et al. (1984) hypothesis, whereby the red-shifted jet is orientated away from the primary molecular cloud, and is sweeping-up relatively small amounts of low-density material.

Such a discussion is, of course, no more than suggestive, and the application of LVG modelling is intended as purely illustrative – although the general trends deduced above are almost certainly valid. Further and more detailed analysis will require observations of the CO isotopes, and a more extensive mapping of the redward flow.

Finally, the CO $J=3-2$ results have been summarised in Fig. 13, where we illustrate the decline in T_R^* from the source centre, the variation of the FWHM (a parameter which appears to peak north of the source at these frequencies), and the distribution of red and blue wing emission at the centre. The limited sampling area of the data results in a very restricted separation of the outflow lobes, and the red and blue wings appear, indeed, to be almost co-spatial, as noted by Lada et al. (1984). The central collimation for this source must therefore be either extremely poor, or correspond to an orientation which is close to the line of sight – and therefore different from that of the more extended flow lobes.

Also noteworthy is the relatively rapid fall-off in peak values of T_R^* from the source centre. This, of itself, can be used to place reasonably tight constraints upon the local mean density and mass, providing local kinematic stability is assumed. For thermal stability, for instance, we find that the limiting density is given by

$$n_m \sim \frac{8.8\,10^2\,T_k}{(D/\mathrm{kpc})\,(d/1\,\mathrm{arcmin})}\,\mathrm{cm}^{-3},$$

where D is the source distance, and d is the diameter. The corresponding mass is given through

$$(M/M_\odot) \sim 0.56\,T_k\,(D/\mathrm{kpc})\,(d/1\,\mathrm{arcmin}),$$

whence for $d \sim 2$ arcmin, and $D \sim 1.5$ kpc (Wendker and Baars, 1974) we determine $n_m \sim 2.4\,10^3\,\mathrm{cm}^{-3}$, and $M \sim 42\,M_\odot$. Under conditions of thermal, rotational and pressure equilibrium we also find however that

$$\frac{X(CO)}{dv/dr} \sim 3.4\,10^{-3}\,n(H_2)^{-1/2}\ \ \mathrm{km^{-1}\,s\,pc}$$

a relation which also very broadly applies where free-fall collapse is occurring. As a result, we would expect a value $X(CO)/dv/dr$ which is reasonably modest, and $> 10^{-5}\,\mathrm{km\,s^{-1}\,pc^{-1}}$ for $n(H_2) \lesssim 10^5\,\mathrm{cm}^{-3}$. Detailed LVG analysis of the $J=3-2$ and $J=1-0$ lines however suggests that densities and abundance/velocity gradient ratios are more likely to be of order $\log n(H_2) \sim 4.4 \pm 0.2$, and $\log(X(CO)/dv/dr) \simeq -6.0 \pm 0.3$, which (if true) would imply a rather severe departure from a wide range of stable and nonstable kinematic solutions. It is possible, therefore, that the kinematics and structure of the line core emission zone is strongly determined by the outflow source.

6. W3

As in many of the regions considered in this paper, W3 is a complex mix of molecular and ionised material driven by star-forming activity, although the combination of high velocity flows, self-absorption, and multiple velocity components makes interpretation peculiarly difficult. Details of the overall cloud structure have been considered by Dickel et al. (1980), Lada et al. (1978), and others whilst the most recent observations include those of the C90α recombination line (Jaffe and Wilson, 1981), 400 μm continuum mapping by Jaffe et al. (1983), mapping of HCO^+ by Sandqvist et al. (1982, 1983), observations of H_2CO by Arnal et al. (1982), and high resolution HCN aperture synthesis mapping by Wright et al. (1984). The extensive literature of CO observations includes work by Loren (1981), Brackman and Scoville (1980), Lada et al. (1978), and Dickel et al. (1980). Most recently, Thronson et al. (1985) have modelled the region in terms of the interaction of an H II region, W4, with a previously quiescent CO cloud, extending now to the west of the primary star-formation centres. Such an explanation has considerable merit in explaining the drift of line velocities with spatial position and, in particular, the trend in velocities between the main condensations [W3

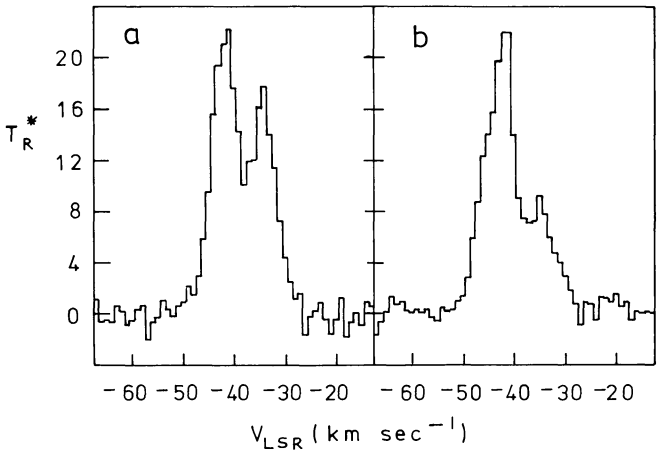

Fig. 14. CO $J=3-2$ profiles of W3 for a) 20″ W, 12″ S of IRS 5; and b) 13″ E, 17″ S of IRS 4

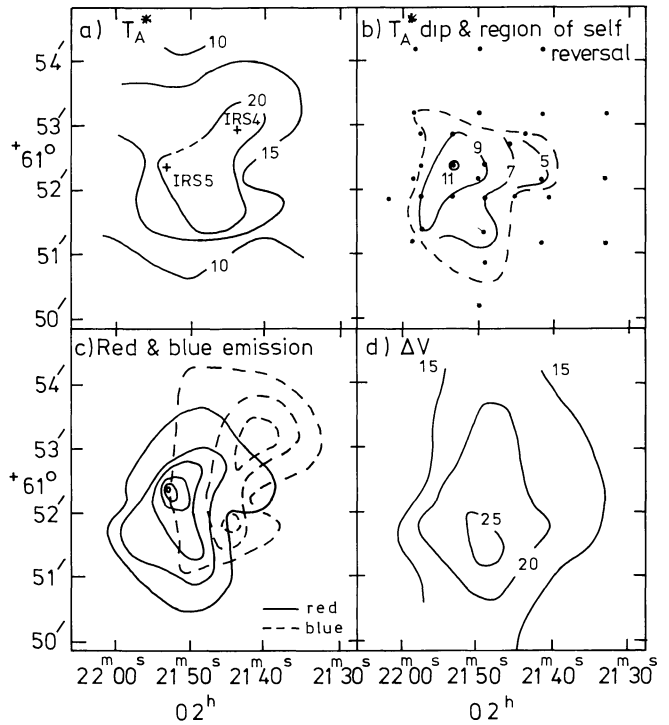

Fig. 15. CO $J=3-2$ variation in T_R^* (peak), T_R^* (dip), line width ΔV (km s^{-1}), and the integrated red ($-33 \leqq V_{LSR} \leqq -25$ km s^{-1}) and blue ($-53 \leqq V_{LSR} \leqq -47$ km s^{-1}) wing emission distributions in W3. The lowest contours take a value 10 K km s^{-1}, with subsequent contours incrementing by 10 K km s^{-1} in both cases

North, W3, W3 (OH) and AFGL 333 in the parlance of Thronson et al.], all of which are presumed to be on the semi-spheroidal interface between the molecular cloud and W4. Adjacent quiescent gas, on the other hand, appears to take a velocity $V_{LSR} \sim -42$ km s^{-1}, some 2 km s^{-1} less than for the main neutral condensations and associated ionised gas (Thronson et al., 1982).

The W3 core is associated with an infrared cluster, described and measured by Wynn Williams et al. (1972). The main mass appears to have a velocity $V_{LSR} \sim -40$ km s^{-1}, with T_R^* (CO) peaking at IRS 5, and there is also some evidence for extended self-absorption to the west of IRS 5 (Thronson et al., 1983). Several authors (cf. Sandqvist et al., 1982, 1983) have also noted a second mass component at $V_{LSR} \sim -43$ km s^{-1} apparently associated with IRS 4, and detected in ^{12}CO, HCO$^+$, and ^{13}CO. Sandqvist et al. (1982, 1983) attribute a broad linewidth about $\alpha(1950) = 2^h21^m51^s.0$, $\delta(1950) = +61°52'18''$ to the close proximity of IRS 4 and IRS 5, and therefore of the two cloud components, and there is little doubt that this is a strong factor in explaining the observed kinematics; there is little to justify an explanation in terms of high velocity outflows over large spatial scales, apparently favoured by Thronson et al. (1985). Confusingly, however, it is also clear [from the high resolution work of Claussen et al. (1984)] that IRS 5 is indeed associated with a high velocity outflow, with integrated wing intensities peaking close to the outflow source. Within a short spatial distance, therefore, there appears evidence for both high velocity flows *and* separate velocity mass components.

We have mapped a $4' \times 4'$ area of the W3 cloud core in CO $J=3-2$, centred on the position RA (1950) $= 2^h21^m53^s.2$, DEC (1950) $= +61°51'21''$. Figure 14a shows the line profile 20″ west and 12″ south of IRS 5, whilst Fig. 14b shows the line profile 13″ east and 17″ south of IRS 4. Both profiles reveal strong self-absorption at 37 km s^{-1}, and the area where self-absorption dips are observed is further delineated in Fig. 15. The limits to this region are primarily determined by shifts in emission line widths and central velocities, rather than variations in the cooler foreground cloud.

As in many other sources, the $J=3-2$ self-absorption feature appears to be significantly more pronounced than at lower frequencies; a characteristic usually attributed to low densities in the absorbing material, as discussed earlier. The central dip temperature varies somewhat over the measured region, declining to ~4 K in the south-west, although over most of the source it takes a characteristic temperature $T_{DIP}(J=3-2) \simeq 8$ K. At $J=2-1$ and $J=1-0$, by way of contrast, the value of T_{DIP} appears to be of order ~15 K (cf. Loren, 1981; Phillips et al., 1979). Given that this is one of the few sources to show ^{13}CO self absorption (Thronson et al., 1985), it is clear that the ^{12}CO absorption optical depth is likely to be quite large, for which circumstance we may show that $n(H_2)$ is $\sim 10^3$ cm^{-3} [where we have again assumed $X(CO) \sim 5\ 10^{-5}$, and taken $dv/dr = 1.3$ km s^{-1}].

For a column density $N(^{13}CO) \sim 0.5 - 2\ 10^{16}$ cm^{-2} (Thronson et al., 1985), it then follows that the absorbing region must have an overall thickness ~3–12 pc. The W3 emission core underlying this layer, for comparison, appears to have a diameter of order ~8 pc.

The velocity width is extremely broad close to IRS 4 and IRS 5, as noted by other investigators (see earlier). This we believe can be entirely attributed to the superposition of two cloud components at differing velocities (cf. Sandqvist et al., 1983), and support for this is also provided in Fig. 15, where we have plotted both blue- and red-wing distributions. The red wing ($-33 < V_{LSR} < -25$ km s^{-1}) is clearly seen to take a maximum near IRS 5, whilst blue shifted emission ($-53 < V_{LSR} < -47$ km s^{-1}) is alternatively centred on IRS 4.

Given, however, that the bulk of the W3 mass is at $V_{LSR} \simeq 39$ km s^{-1}, and is presumably driven by W4, then we may reasonably ask why a separate condensation (IRS 4) is present at $V_{LSR} \sim 43$ km s^{-1}; a result which is not obviously explainable through the simple model described above.

Such a query has also been addressed by Thronson et al. (1985), although without any evident conclusion. From their more

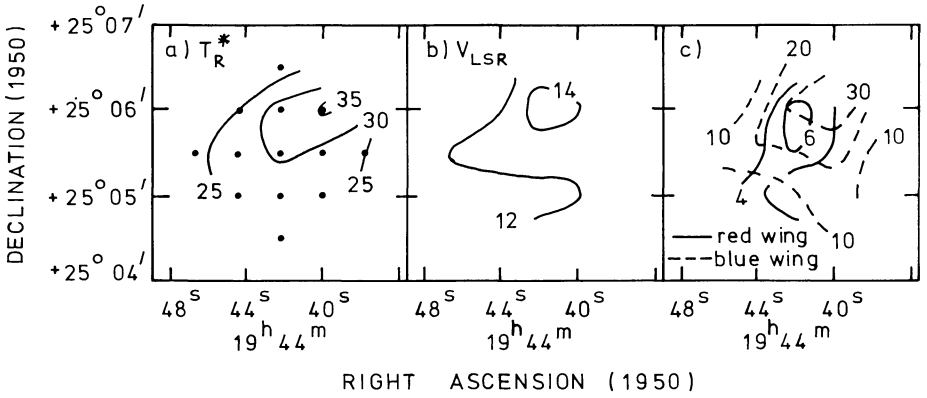

Fig. 16. CO $J=2-1$ variations of T_R^* (peak), central line velocity V_{LSR} (km s^{-1}), and red ($28 < V_{LSR} < 32$) km s^{-1}) and blue ($15 < V_{LSR} < 19$ km s^{-1}) wing emission distributions (K km s^{-1}) for S88

widespread mapping of this region in CO $J=1-0$, however, we note that the velocity of the IRS 4 cloud is very similar to that of the immediately adjacent quiescent material – the IRS 4 cloud is kinematically and spatially associated with a region which, supposedly, is undistrubed. Precisely how star-formation could be triggered in advance of the W4 shock is rather unclear – although a possible explanation may centre on the nearby source IRS 5. This, as we have noted, is the focus of considerable kinematic activity, with evidence for outflow along an east-west axis. It is possible, therefore, that material from this source is directly impinging upon the material west of IRS 5, leading to local instability and collapse in advance of the star-formation zone. This would certainly prove an interesting hypothesis, a reverse of the dispersive properties usually attributed to these flows, although such a process can at present be regarded as no more than speculative. Further, and in particular, more extensive high resolution observations of this region would be extremely welcome.

7. S88

The S88A nebula takes the form of a low emission measure H II region located at a distance of 2 kpc (Lortet-Zuckermann, 1974; Evans et al., 1981; Blitz et al., 1982). The region has been investigated at radio wavelengths by Felli and Harten (1981), who find the predominant emission to arise in a multicomponent compact core obscured by perhaps 40 mag of foreground extinction. The far-infrared emission appears to be co-centric with the radio source, although more extended, whilst the near infrared emission is located closer to the Hα emission zone (Evans et al., 1981). This displacement between emission peaks has been met elsewhere in this paper, in the case of K3-50, where it was attributed to strongly varying differential extinction across an edgewise blister zone. Some such similar explanation also appears to be appropriate here (cf. Evans et al., 1981; Felli and Harten, 1981). CO $J=1-0$ measures by Evans et al. (1981) reveal a compact ($\sim 8'$ diameter at FWHM) neutral cloud centred on the radio source, although no evidence was found for appreciable levels of H_2CO emission, implying that densities cannot greatly exceed $\sim 10^5$ cm^{-3}. Optical estimates of the electron density n_e, on the other hand, appear to imply values of order $\sim 10^4$ cm^{-3}, suggesting that neutral cloud densities cannot be uniformly low.

The present observations examine the distribution in S88 of CO $J=3-2$ and $J=2-1$ emission. A total of forty one positions were observed in the $J=3-2$ line, in most cases spaced at half-beamwidth intervals, whilst a more limited sample of 13 spectra were acquired in $J=2-1$. The $J=2-1$ CO results are summarised in Fig. 16, whilst the more extensive $J=3-2$ data set is illustrated in Fig. 17, together with a range of comparative optical and radio mapping results.

The $J=3-2$ temperature peak lies approximately 30″ east of the reference position, and is coincident with the FIR peak of Evans et al. (1981), although it drops away to half this intensity within a distance of 1′.7. Similar variations are to be found at $J=2-1$, with the temperature peak lying in this case a little further to the west – although differences between the maps are slight, and may not be significant. The variation of V_{LSR} at T_R^* (peak) is provided in panel 17c, and it is clear from this that, at $J=3-2$ at least, there is a regular drift in line velocity along a NE-SW axis. The value of the full line width V_{max}, on the other hand, appears to have a more complex distribution, although peak values again appear to be centred close to the reference location (Table 1).

The change of T_R (peak) with right ascension is further illustrated in Fig. 18, where we include both $J=2-1$ and $J=3-2$ results. The comparative $J=1-0$ results of Evans et al. (taken with the MWO and NRAO facilities) are, however, somewhat more problematic. An MWO $J=2-1$ spectrum taken 30″ north, 1′ east of the reference position, for instance, displays a temperature $T_R \sim 50$ K greatly in excess of the line values presented here, and a profile which is distinctly at variance with the rather innocuous line shapes obtained here (and typically represented in Fig. 19). Neither of these discrepancies is entirely comprehensible in terms of differing beam sizes, and a direct comparison with our data proves impracticable.

In analysing their results, however, Evans et al. (1981) arbitrarily increased their Kitt Peak temperatures by $\sim 30\%$ to achieve consistency with the MWO spectra, and it is clear that at least one of the data sets must be in error.

For the purposes of comparison with our $J=3-2$ and $J=2-1$ results, we find that their Kitt Peak (rather than MWO) calibration appears the more consistent. We have therefore re-calibrated their $J=1-0$ map of this source to the Kitt Peak standard in comparing the peak temperature variations in Fig. 18.

If this is accepted (and the alternative MWO solutions would certainly be inconsistent with our data), then it is possible to make an appropriate assessment of the density variation through the source. For this purpose we have used an LVG analysis to match the $J=3-2$, $J=2-1$, and $J=1-0$ line intensities. The kinetic temperature is presumed to vary as, and to be congruent with $T_{ex}(J=1-0)$, the $J=1-0$ excitation temperature, whilst the velocity gradient dv/dr is taken to be 1.2 km s^{-1} pc^{-1}; similar to values found in other dark clouds, and consistent with the gradient

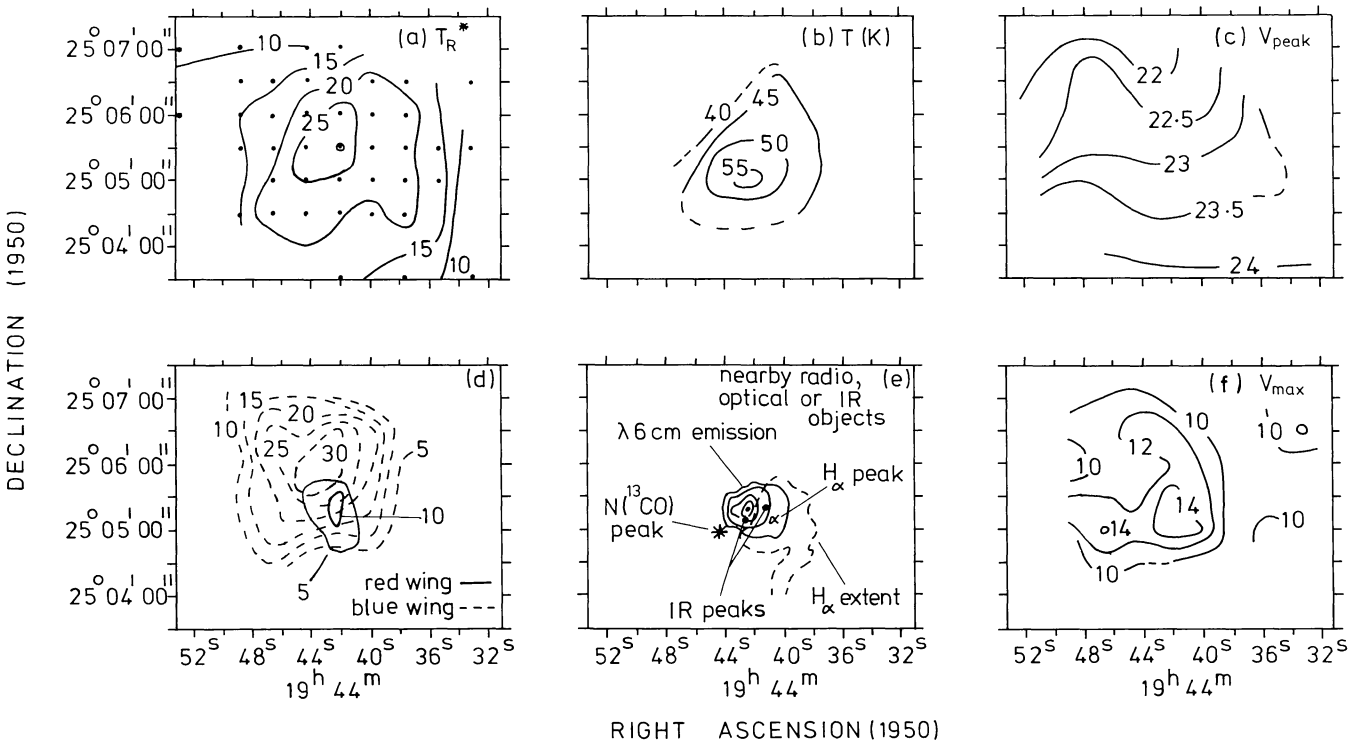

Fig. 17. Variation of a range of CO $J=3-2$, optical, FIR, and radio parameters in S88. The variation of dust temperature T(K), and radio and optical emission distributions derives from Evans et al. (1981). The central line variation of V_{LSR} is provided in panel (c), whilst the maximum line width at the $T_R^* = 1$ K level is denoted by V_{max} (panel f). The wing integrals in panel (d) correspond to the same velocity ranges as for Fig. 16

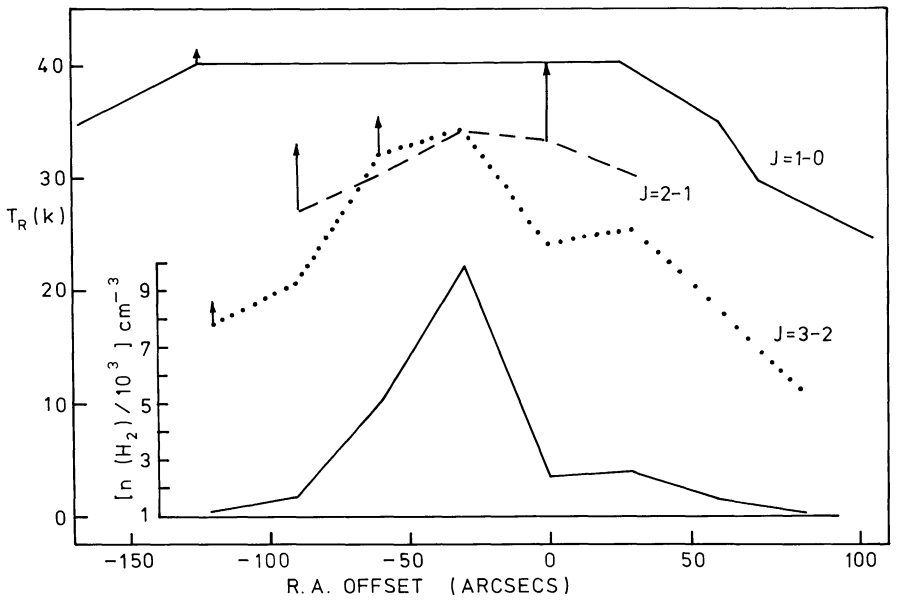

Fig. 18. Variation of $T_R(J \rightarrow J-1)$ for an R.A. traverse through S88 ($\delta = 25°05'30''$). The zero offset corresponds to the reference R.A. in table 1 whilst vertical arrows indicate the corrections required for T_B. Also illustrated is the variation of $n(H_2)$ derived through an LVG analysis; maximum densities appear to exceed $\sim 10^4\,cm^{-3}$, and are centred close to the extincted radio source.

in peak line velocities noted in Fig. 17. We similarly assume an invariant molecular fraction $X(CO) \simeq 5\ 10^{-5}$, again comparable to values found in other dark clouds.

Finally, the results have been weighted to yield approximate brightness temperatures, T_B, calculated on the assumption that the source diameter is $D = 3'$ at $J=2-1$ and $J=3-2$, and $8'$ at $J=1-0$. This value of $D(J=2-1)$ is possibly a lower limit, although the uncertainties are not such as to greatly affect this analysis. As a result, we find that central values of T_B/T_R are of order $\sim(1+(B/D)^2)^{-1} \sim 1.21$ at $J=2-1$, and ~ 1.19 at $J=3-2$, where B is the beam FWHM. The increase of T_B over T_R at $J=1-0$ is almost negligible, of order 2%.

The resultant derived values of $n(H_2)$ are illustrated in Fig. 18. Whilst such an analysis is clearly only suggestive, the general features to emerge are surely quite accurate. In particular, much of the cloud is likely to require a quite low density to explain the

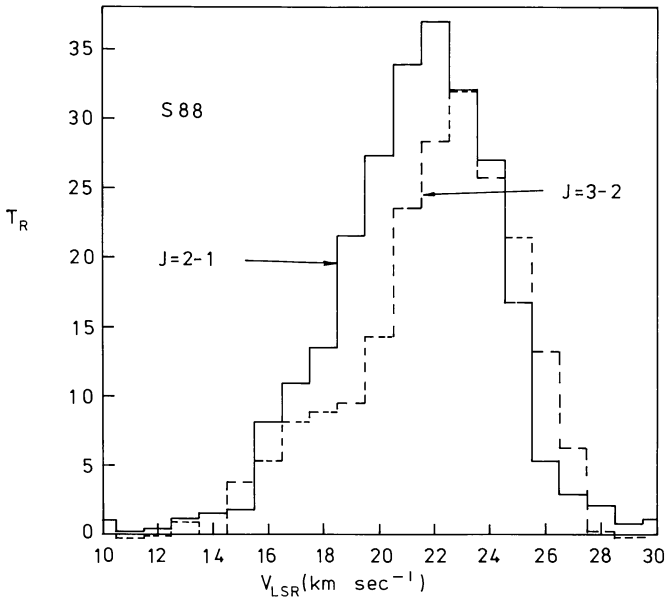

Fig. 19. Comparative $J=3-2$ and $J=2-1$ CO spectra for S88, taken at the [0,0] reference position

disparity between $J=3-2$ and $J=2-1$ line intensities, although the similarity of $J=2-1$ and $J=3-2$ brightness temperatures at the core requires a density $\gtrsim 10^4\,\mathrm{cm}^{-3}$. The position of the density peak, between 30″ and 60″ east of the reference position, falls directly upon the compact radio core.

Further evidence for extensive activity centred on the radio/FIR core is provided in Figs. 16 and 17, where we plot the distribution of red ($28 < V_{LSR} < 32\,\mathrm{km\,s}^{-1}$) and blue ($15 < V_{LSR} < 19\,\mathrm{km\,s}^{-1}$) wing emission. It appears, from this, that S88 represents another example of a bipolar outflow source, although the red wing is barely resolved. The blue wing, on the other hand, extends over a region with diameter $\sim 2'$, and appears to be only poorly collimated. Whilst there are again small differences in the wing distributions at $J=2-1$ and $J=3-2$ – the $J=2-1$ red wing appears to possess a slightly different orientation to that at $J=3-2$ – the agreement is by and large reasonably close; and in particular, the relatively compact dimensions of the red outflow is confirmed at both frequencies. A direct comparison of $J=2-1$ and $J=3-2$ line profiles for the 0.5 E 0.5 N position is provided in Fig. 19. Such a comparison should, of course, be viewed with caution; the beam sizes are quite different, and this is likely to result in kinematic differences as differing regions of the source are sampled, and different levels of dilution apply. In general, however, and given the central values of $T_B/T_R(J)$ quoted earlier, it is likely that $T_B(J=2-1)/T_B(J=3-2)$ is >1.5 for the blue wing at least. This would in turn imply $\log n(\mathrm{H_2}) \lesssim 3.0$ for $T_k = 40$ K, and $\log(X(\mathrm{CO})/dv/dr) \gtrsim -8$, or $\log n(\mathrm{H_2}) \lesssim 3.0$ for $\log(X(\mathrm{CO})/dv/dr) \gtrsim -4.5$. The intensities at $V_{LSR} = 18\,\mathrm{km\,s}^{-1}$, appropriately corrected for beam dilution (see earlier), yield the more specific solution $\log(X(\mathrm{CO})/dv/dr) \simeq -5.50 \pm 0.5$, and $\log n(\mathrm{H_2}) \sim 3.3 \pm 0.3$, although it would seem that $T_R(J=2-1)/T_R(J=3-2)$ declines towards lower velocities (where the S/N unfortunately also retreats), suggesting that higher mass densities may be relevant away from the core V_{LSR}. For the red wing, on the other hand, there appears evidence that $J=3-2$ emission may even be stronger than at $J=2-1$, and this would in turn imply exceptionally high densities ($n(\mathrm{H_2}) \gtrsim 10^5\,\mathrm{cm}^{-3}$), and correspondingly large velocity gradients. Such a conclusion would also be consistent with the observed source morphology, suggesting high red-wing compression and limited spatial expansion, compared to the very much lower density (and more widely distributed) blue wing component. Given however the low velocity resolution, differing beam sizes, and the rather severe effects of slight relative velocity shifts, it is clear that further observations of this critical velocity régime are necessary prior to a more extensive analysis.

For the present, it would seem that much of the extended outflow zone can probably (and rather conservatively) be bracketed in the density range $10^3 < n(\mathrm{H_2}) < 10^4\,\mathrm{cm}^{-3}$, implying outflow energies between $\sim 3\ 10^{45}$ erg and $3\ 10^{46}$ erg (assuming a mean flow velocity of $\sim 6\,\mathrm{km\,s}^{-1}$, and corresponding dynamical timescale $7\ 10^4$ year), values which are entirely in line with other bipolars (cf. Lada, 1984). The outflow momentum similarly resides between $48\,M_\odot\,\mathrm{km\,s}^{-1}$ and a value ten times as large – a range which lies comfortably within the bracket of observed HVMOs. More useful constraints upon these parameters will require reliable observations in other transitions (cf. $J=1-0$), and other CO isotopes.

Finally, the nature of the velocity shift noted in Fig. 17c is not entirely clear, although if attributed to cloud rotation would imply a mass $2\ 10^2\,M_\odot$ for the central 3′ diameter core zone. Extrapolating to the CO $J=1-0$ diameter of 8′, and assuming a similar velocity gradient to apply there also, would then yield an overall cloud mass $\sim 4\ 10^3\,M_\odot$ – assuming, of course, that the cloud is in rotational equilibrium. This, in turn, can be shown to imply a mean $\mathrm{H_2}$ density $n(\mathrm{H_2}) \sim 1.5\ 10^3\,\mathrm{cm}^{-3}$; comfortably in agreement with the values determined in figure 18 from LVG modelling, although the overall extinction [~ 22 mag if $A_v/N(\mathrm{H_2}) \sim 10^{-21}$ mass] would be lower than Felli and Harten (1981) estimate to the radio source. It appears possible, therefore, that the primary (lower density) cloud mass is close to rotational equilibrium. Much of the extinction in front of the radio source must however derive from a higher density core zone which is barely resolved in the present results, and may not be rotationally stabilised.

To summarise, therefore, it appears that the S88 radio core is located close to a similarly compact high density neutral zone. Whilst densities $n(\mathrm{H_2})$ appear not to exceed $\sim 10^5\,\mathrm{cm}^{-3}$ (cf. Evans et al.), they can hardly be very much lower than $\sim 10^4\,\mathrm{cm}^{-3}$. A low velocity blue wing appears to extend over much of the core, and is relatively uncollimated, whilst the red wing appears to be extremely compact. This bipolar source also appears to be located very close to the main radio peak.

8. NGC 2264

The extremely young cluster NGC 2264 is located in a region of continuing star formation, H II regions, and molecular clouds, the whole forming a complex structure whose properties are far from well established. The most distinctive optical structure in this region is the cone nebula, an apparent wedge-shaped shadow zone extending behind a box-shaped globule, although the illuminating source for this object is far from being well established; Schwartz et al. (1985) argue in favour of S Mon, whilst earlier investigators noted that IRS 1, a strong obscured infrared source, is located at the projected apex of this structure (Allen, 1972). For either case, however, it is clear that the cone nebula is far less important for the structure of this region than its optical appearance might suggest; there is little evidence for it in the molecular line or FIR continuum

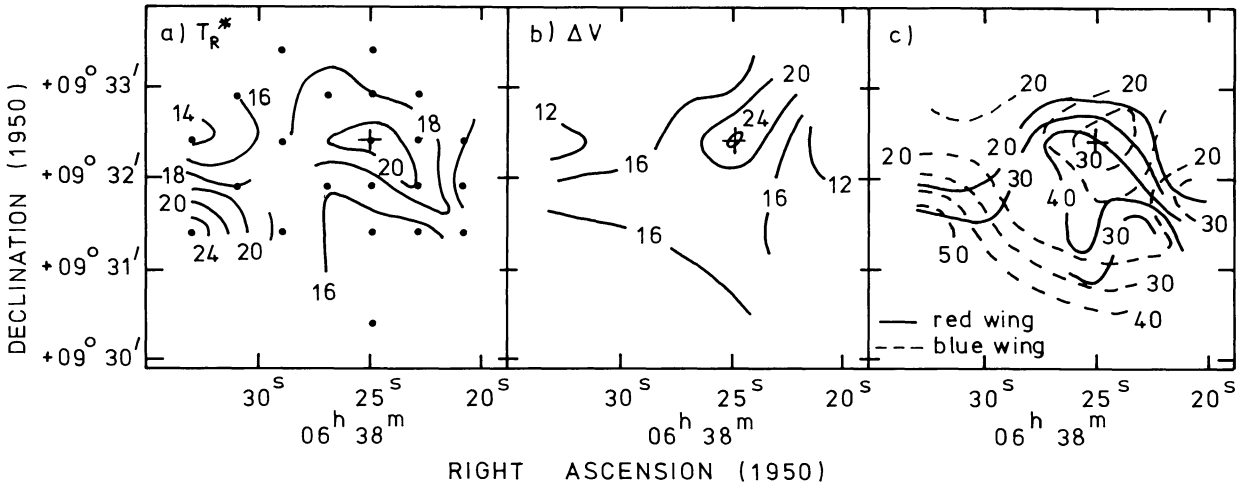

Fig. 20. CO $J=3-2$ variation in peak line temperature T_R^* (peak), full line width at the $T_R^*=1$ K level, and integrated red ($12 \leqq V_{LSR} \leqq 24$) and blue ($-8 \leqq V_{LSR} \leqq 4$) wing emission distributions (K km s^{-1}) for NGC 2264

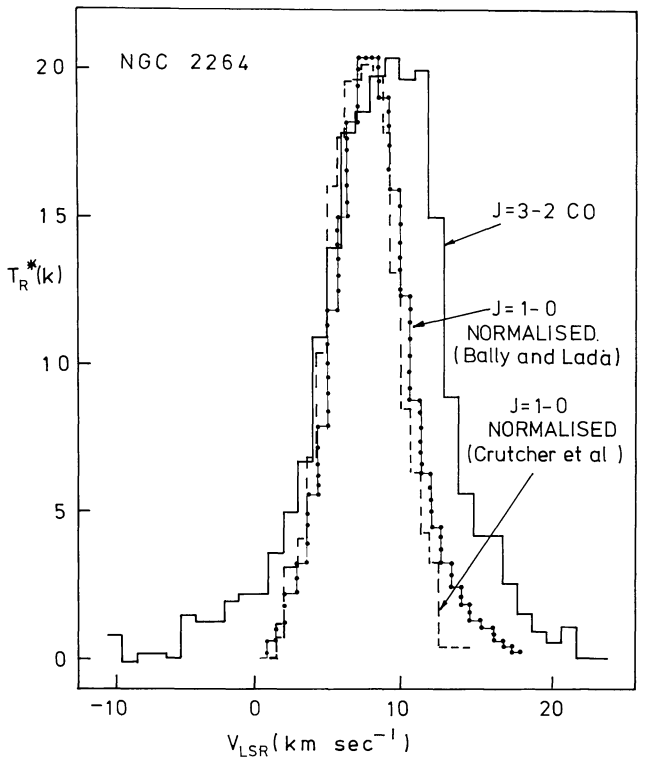

Fig. 21. Comparison of $J=1-0$ and $J=3-2$ CO spectra for the [0,0] reference position in NGC 2264 (Table 10). The $J=1-0$ results derive from Crutcher et al. (1978; ----) and Bally and Lada (1983; ....), and have in both cases been normalised to the $J=3-2$ peak antenna temperature

mapping results of Schwartz et al (1985) and Crutcher et al. (1978), for instance. The region about IRS 1 appears, however, to locate a higher density molecular core within a more extensive CO envelope. The kinematic structure of CO in this region is highly variable over short spatial scales, and appears to testify to a variety of molecular structures, not all of which are necessarily related. Systematic velocity trends in the vicinity of IRS 1, however, suggest it to be located in a rotating molecular toroid of diameter $\sim 30'$ (Crutcher et al., 1978). The spectral type of IRS 1 is, again, a matter of some debate (cf. Harvey et al., 1977; Thompson and Tokunaga, 1978) with a range of contradictory and confusing evidence leading to differing conclusions. The overall radio and infrared fluxes are consistent however in implying a B3V ZAMS or similar star (Schwartz et al., 1985).

Bally and Lada (1983) found CO velocities near IRS 1 to be large, of order 28 km s^{-1} at the 100 mK level, and Schwartz et al. (1985) have subsequently mapped a red-wing extending south of the source, a structure they attribute to a blister-like formation at the edge of the toroid. Our additional $J=3-2$ CO results map a region 6 arcmin^2 about this source, and the details are summarised in Fig. 20. The CO emission peaks at the infrared source, although it is interesting to note that the emission structure is extended orthogonally to the CO ridge found by Crutcher et al. (1978), and parallels the high density molecular tracers such as CS (cf. Schwartz et al., 1985). There is also evidence (based primarily upon three spectra) for a rapid temperature increase to the south east of the reference position (Table 1). The most interesting result to emerge from the present data, however, is the presence of a blue wing to the north-west of the source. It would appear, in short, that NGC 2264 may possess a bipolar configuration, as opposed to the monopolar structure discussed by Schwartz et al. (1985). If this were true, of course, then the model of Schwartz et al. could hardly also be applicable to this source, although it is wise to counsel some caution at this stage. Several other negative velocity zones are scattered about this region, as noted in Fig. 20, and the location of the blue wing may be quite fortuitous. Further observations at higher resolution would be greatly welcomed.

This said, however, we may question why a similar wing was not noted by Schwartz et al. The answer to this question is not clearly answerable at present, since Schwartz et al. have yet to publish their $J=1-0$ spectra. A comparison of our $J=3-2$ data with $J=1-0$ spectra taken with larger beams, however, offers a possible explanation. For this purpose, we have taken the 7m Bell Labs $J=1-0$ spectrum of Bally and Lada (1983) together with the 4.6m Aerospace Corporation $J=1-0$ results of Crutcher et al. (1978), and overlaid these onto our $J=3-2$ CO spectrum for NGC 2264 IRS 1 (Fig. 21). The temperatures have in all cases been normalised to the T_R^* ($J=3-2$) scale; a comparative derivation of T_R would be unreliable with the available beam parameters.

Despite the large beam differences, the Crutcher et al. and Bally and Lada $J=1-0$ results are very closely similar – excepting

an extended wing in the Bell Labs data between $11 \lesssim V_{LSR} \lesssim 15\,km\,s^{-1}$. The beam size of the present $J=3-2$ results bears roughly the same relation to the Bell Labs beamsize, as the Bell Labs beam bears to that of Crutcher et al. The spectral differences however are far more remarkable. For this case, the $J=3-2$ emission appears to extend to $V_{LSR} \sim -5\,km\,s^{-1}$ (a régime over which there is no appreciable $J=1-0$ emission), and the red wing is massively enhanced. Whether this reflects beam dilution effects alone cannot at present be answered, although there is a strong hint that much of the gas may be optically thin. The emission between $-5 < V_{LSR} < 0\,km\,s^{-1}$, for instance, is between 10 and 20 times greater at $J=3-2$ than appears to be the case in the $J=1-0$ spectrum of Bally and Lada; a result which can hardly reflect beam dilution effects alone [unless, of course, T_R (peak) at $J=3-2$ is considerably less than at $J=1-0$]. If this is the case, therefore, then the absence of appreciable blue shifted components in the data of Schwartz et al. (1985) might be easily understood. Such a trend would also tend to imply low densities ($\sim 10^3\,cm^{-3}$), high velocity gradients, or both.

The results presented here therefore appear to be both interesting and suggestive, although further comparative (lower and higher frequency) mapping would be of considerable help in interpreting these trends.

9. NGC 1333 (HH7-11)

The NGC 1333 molecular cloud appears to be part of a much larger complex associated with the Perseus OB2 association (Sargent, 1979). Evidence for star-formation is extensive, and includes multiple, highly extincted infrared sources (Strom et al., 1976), H_2O maser emission (Haschick et al., 1980), Herbig-Haro objects, T-Tauri stars and Hα emission stars (Herbig, 1974; Strom et al., 1974), and high velocity molecular outflows (Snell and Edwards, 1984; White et al., 1980). At millimetre wavelengths, observations by Lada et al. (1974) revealed the presence of H_2O, CS, and HCN emission southwest of the optical nebula, and both CS and NH_3 peak close to the infrared source 13 of Strom et al. (1976), hereafter referred to as HH 7-11 (IR). The region has been extensively mapped in CO $J=1-0$ by Loren (1976), who proposed that much of the star-forming activity was triggered by colliding clouds; an interpretation which was subsequently queried by Ho and Barrett (1980) on the basis of NH_3 observations. More recent CO mapping includes the $J=3-2$ work of White et al. (1981), who investigated a large ($10 \times 6\,arcmin^2$) region centred on HH 7-11 IR, and revealed the presence of at least two primary condensations centred close to the infrared source. A comparison of their $J=3-2$ spectrum with a $J=1-0$ MWO profile suggested quite severe variations in spectral line shape, and the possibility of optically thin wing emission. Such departures in line profile were also confirmed by Snell and Edwards (1981) at $J=1-0$ and $J=2-1$, together with the presence of extensive and spatially separated red- and blue-wing components. The wing temperature ratios between $J=2-1$ and $J=1-0$ were also found to be large, and consistent with excitation temperatures $T_{ex}(1-0) \sim 10 \rightarrow 25\,K$, whilst the overall mass of red and blue shifted gas was estimated at $\sim 4.2\,M_\odot$.

Our present observations consist of a further 6 CO $J=3-2$ spectra taken close to HH 7-11 IR, and coincident with the positions of six $J=2-1$ spectra illustrated by Snell and Edwards (1981, Fig. 3). The spectra, together with those of Snell and Edwards (1981), are illustrated in Fig. 22 (note the difference in temperature and velocity scales). As a consequence, it is immedi-

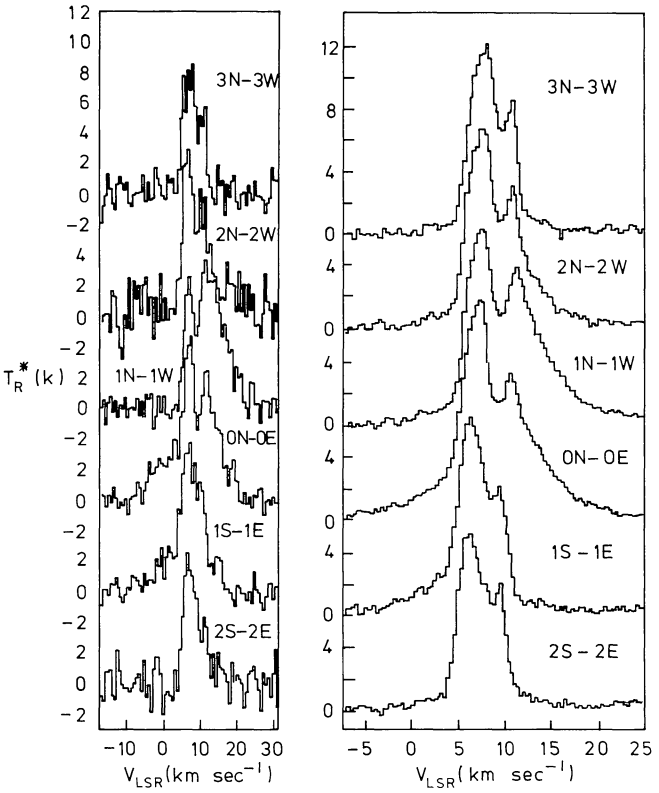

Fig. 22. CO $J=2-1$ and $J=3-2$ spectra for six locations near NGC 1333 (HH 7-11). The offset positions are with respect to the reference locations in table 1, and the $J=2-1$ data derives from Snell and Edwards (1981). Note the differences in velocity and temperature scales between the $J=3-2$ and $J=2-1$ results

ately apparent that although our present S/N is less than that of the $J=2-1$ data, the profile shapes are notably different. The self absorption feature at $V_{LSR} \sim 9\,km\,s^{-1}$, for instance, is quite clearly deeper at $J=3-2$ than at $J=2-1$, a characteristic noted elsewhere in this paper for other sources. In the present case, however, it is apparent that the assumption of differing absorption/emission zone excitation properties, and in particular, reduced absorption zone densities, is only partly capable of explaining these trends. In fact, and as noted by Snell and Edwards (1981), it is clear that the underlying emission is varying quite rapidly with transition $J \rightarrow J-1$, broadening as the frequency increases, and thereby accentuating the apparent depth of the absorption feature. Snell and Edwards (on the basis of $J=1-0$, $J=2-1$, and our earlier $J=3-2$ results) attributed these variations to optically thin CO emission, a presumption which is supported by the small limiting wing ratios $T_A^*(^{13}CO)/T_A^*(^{12}CO) < 0.012$. Our present results suggest that the wings continue to gain prominence at $J=3-2$ CO, at the expense of the more widespread $V_{LSR} \sim 7\,km\,s^{-1}$ line component, so that the $J=3-2$ and $J=2-1$ line profiles are only broadly comparable near HH 7-11 IRS.

A more direct comparison of spectra at HH 7-11 IRS is provided in Fig. 23, where we have plotted our own $J=3-2$ spectra, together with the $J=1-0$ and $J=2-1$ spectra of Snell and Edwards (1981). For the $J=1-0$ spectrum, taken with the 14m FCRAO telescope (beam size 50″) we have taken $\eta_c \times \eta_{fss} \sim 0.36$, whilst for the $J=2-1$ results, taken with the 4.9m MWO (beamsize 1′.3) we take $\eta_c \times \eta_{fss} \simeq 0.43$ (a little less than the value 0.45 quoted by Snell and Edwards). The beamsizes, in short,

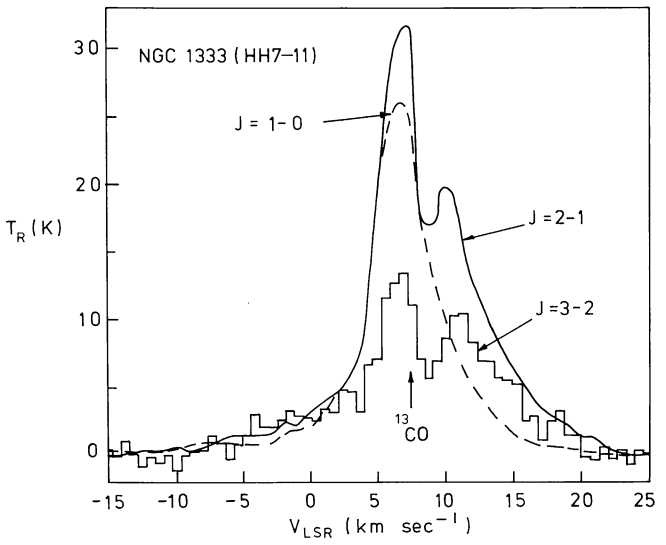

Fig. 23. CO $J=3-2$, $J=2-1$, and $J=1-0$ spectra for the [0,0] reference position in NGC 1333 (HH7-11). The $J=2-1$ and $J=1-0$ results are adapted from Snell and Edwards (1981)

are not too dissimilar, and large variations in spectral profile are unlikely to depend upon beam dilution. The beam dilution is almost certainly a strong function of V_{LSR}, on the other hand, with $W_{BLUE} < W_{RED} < W_{CORE}$. The variation of *brightness* temperature $T_B(V_{LSR})$, therefore, is almost certainly quite different from that of $T_R(V_{LSR})$, and the observed line profiles.

Many of the details evident in Fig. 22, and discussed above, are very clearly demonstrated in Fig. 23. In addition, it is clear that the $J=3-2$ profile is substantially weaker at the core ($V_{LSR} \sim 8\,km\,s^{-1}$) than for either $J=2-1$ or $J=1-0$, taking a typical value ~ 0.42 ($J=2-1$). Towards the wings however, this disparity becomes smaller, and it is possible that $T_R(J=2-1)$ and $T_R(J=3-2)$ approach parity – a situation which is closely reminiscent of that encountered earlier for S140.

The physical state of the emission zone has already been considered by Snell et al. on the basis of $J=2-1$ and $J=1-0$ spectra. For the present analysis, we have used similar LVG techniques to investigate all three of the CO transitions. We assume, as elsewhere in this paper, that beam dilution is the same at all three frequencies – a situation which is likely to pertain providing that optical depths $\tau(J \rightarrow J-1)$ do not vary from less than unity at certain transitions, to values which are greater than unity at others.

We shall also adopt a kinetic temperature of 40 K, close to the maximum observed radiation temperature [and the corresponding excitation temperature $T_{ex}(J=2-1)$, assuming dilution $W \sim 1$, and $\tau(J=2-1) \gg 1$ at the emission peak]. For these circumstances, however, we find that no solutions are possible for the peak intensities at $V_{LSR} = 7\,km\,s^{-1}$, a situation which is replicated at all other temperatures T_k, and for values of dilution $W < 1$. Expressed in other words, it is apparent that the relevant $J=1-0/J=2-0$ intensity ratio presupposes quite high densities, whilst the high value of $T_R(J=2-1)/T_R(J=3-2)$ indicates quite the contrary. This is not say that a combination of such ratios is impossible per se – a solution can in fact be found for $\log(X/dv/dr) \simeq -8$, and $\log n(H_2) \sim 3.3$. The radiation temperature for such a solution, however, would be of order $\ll 1$ K at all transitions. It is apparent, therefore, that either the present results cannot be modelled by a simple LVG model such as is applied here, or the line intensities T_R are incorrect.

This also appears to be the case at higher velocities. Attempts at modelling line ratios for $V_{LSR} = 11\,km\,s^{-1}$ and $16\,km\,s^{-1}$, for instance, yield essentially negative results.

Given this problem, therefore, we have attempted to model the $J=2-1$ and $J=3-2$ lines alone; transitions for which the profiles are, at least, broadly similar. Here again, however, it proves all but impossible to find a satisfactory solution for the core intensities, irrespective of the value of T_k. The wings, by way of contrast, appear to imply quite high outflow densities, and for $V_{LSR} \simeq 15\,km\,s^{-1}$ we determine a solution $\log n(H_2) \sim 4.2$ and $\log(X(CO)/dv/dr) \sim -7.1$. The close comparability of blue wing emission intensities can also be taken to indicate densities that are reasonably high (for, again, a gas kinetic temperature $T_k = 40$ K).

Precisely why the core intensities between $4 < V_{LSR} < 13\,km\,s^{-1}$ prove so difficult to model is unclear, although it is at least apparent that a simple solution is precluded. Perhaps the apparent self-absorption at $V_{LSR} \sim 9\,km\,s^{-1}$ (see the $J=2-1$ profile) is indicative of a very much broader absorption structure, attenuating the entire line core – in which case excitation densities within the self-absorbing region must be tolerably high. It is unlikely, on the other hand, that the degree of clumping (and therefore beam dilution) can be a strong function of transition frequency, for the reasons enumerated in Sect. 2.

Whatever the reasons for this severe disparity in line strengths, therefore, it seems likely that further observations will be required to determine what seems, in all likelihood, to be a quite complex source structure. Whilst individual line pairs can be modelled, our present results have shown that a simple LVG formalism (coupled to an homogeneous density structure) would be quite inadequate to the task of modelling all three of the transitions considered here.

10. G35.2-0.74

The source G35.2-0.74 appears to consist of an extended cloud with at least two centres of H_2O maser emission, possibly relating to star forming activity. The more southerly maser source was first detected by Little et al. (1983), and recent observations of this region have been reported in CO, ^{13}CO, $H^{12}CO^+$, and NH_3 (Matthews et al., 1984; Little et al., 1983; Brown et al., 1982). All of these molecules have lines possessing a double velocity structure, with components at $V_{LSR} \sim 35.5\,km\,s^{-1}$ and $\sim 32\,km\,s^{-1}$, and the generally symmetric distribution of the line splitting has been taken to imply the expansion of a spheroidal shell (Little et al., 1983).

The more northerly maser source was discovered by Batchelor et al. (1983), and subsequent observations in CS, CO, ^{13}CO, NH_3, HCO^+, and the radio and infrared continua have revealed a complex distribution of structures, the nature and meaning of which are still far from being resolved (Dent et al., 1985; Little et al., 1983; Dent et al., 1985b; Matthews et al., 1984; Dent et al., 1984; Little et al., 1985). ^{13}CO and CO $J=2-1$ observations by Little et al. (1983), for instance, reveal a region in which self-absorption is widespread, and the velocity range ($\Delta V_{LSR} \sim 29\,km\,s^{-1}$) considerable, with many of the profiles showing strong asymmetries. Subsequent mapping of the line wings in HCO^+ indicates that both high and low velocity components are broadly co-spatial (Matthews et al., 1984).

Evidence for bipolarity is at best marginal, with some red-wing enhancement SW of the maser position. This trend is also confirmed, in large part, by the higher resolution CO observations

of Dent et al. (1985), who showed that the red and blue wings were indeed co-spatial, and orientated approximately NE-SW. Furthermore, whilst the wing emission extended in a ridge across the maser source, the primary emission for both wings was located to the NW.

Mapping in CS and NH_3 (Dent et al., 1985b, 1984; Little et al., 1985), by way of contrast, indicates that the higher density gas is concentrated in a rotating toroidal structure, orientated perpendicular to the line of sight and orthogonally to the CO high velocity ridge – a trend which suggests a possible mode of flow collimation. The nature of the outflow source itself, however, is rather less clear. Dent et al. (1985a) find a nearby infrared point source with associated infrared continuum and $H_2S(1)$ $V=1-0$ bipolarity, and this is in turn located between two closely spaced peaks of radio continuum emission. The location of this source outside of the molecular ring, however, together with the differing orientations of the infrared/radio and CO bipolarities, would make interpretation of the CO outflow dynamics peculiarly difficult.

As a consequence, Dent et al. (1985a) have suggested that the star must have drifted away from the molecular ring at a peculiar velocity $\sim 1.5\,\mathrm{km\,s^{-1}}$, whilst a further collimation disk close to the star has precessed by at least ~ 40 degrees. If this is so, then a careful overlay of contour maps suggests to us that the southerly radio peak may arise from the interaction of a stellar wind/ionising radiation field with the edge of the molecular disk, whilst the northerly peak shows a similar interaction at the edge of the CO wind cavity.

In either case, it is apparent from the above that any attempt to construct a model of the region based on simple toroidal collimation is unlikely to succeed. Furthermore, the very basis of this model (that there is a bipolar flow) is by no means unambiguously established – although it would be consistent with the observations if $i < \sin^{-1}(\theta/2)$ (see Sect. 3); that is, the flow is more-or-less transverse to the line of sight. Given that the (collimating?) molecular disk is also orientated nearly edge-on, this by no means an unreasonable presumption.

To further investigate this region at $J=3-2$ CO, we observed 22 spectra centred on the northern maser position and extending over a region 4.7 arcmin^2. The results are illustrated in Fig. 24. It is immediately apparent that most (if not all) of the profiles are strongly self-absorbed, to a degree which is larger than appears to be the case at $J=2-1$. Furthermore, the self-absorption dip temperature is clearly quite regular over much of this zone, and comparable to the peak temperatures of the outerlying profiles, for which velocity widths are also greatly reduced. It appears likely, therefore, that we are observing towards the maser a region of broad lines and vigorous kinematic activity, enclosed within an optically thick, cooler, and kinematically less active cloud. This is in turn responsible for narrow band emission lines at the cloud extremities, and foreground absorption at the cloud centre. A similar structure has been proposed for another of the sources in this paper (W3) by Brackmann and Scoville (1980).

We have acquired a central $J=2-1$ CO profile with UKIRT and this is directly compared with our $J=3-2$ spectrum in Fig. 25. At least two notable features are worthy of comment. First, the blue-shifted emission is quite as strong in $J=3-2$ as it is in $J=2-1$. Given a kinetic temperature $T_K \sim 20$ K comparable to the present peak $J=2-1$ line excitation temperature, we then find $\log n(H_2) > 4.25$, and $\log(X/dv/dr) \lesssim -7$. For the red wing, on the other hand, we find $T_R(J=3-2) < T_R(J=2-1)$, and this leads to a somewhat lower estimated density range $3.75 < \log n(H_2) < 4.25$. In brief, therefore, it appears that the red wing may (all other circumstances being equal) be less dense than the blue wing.

The modelling of the core is rather more problematic, and we refrain from making any detailed assessment of excitation conditions in the present analysis; self-absorption represents an important and rather ill-defined feature of this spectrum, although the strength of $J=4-3$ CO spectra in White et al. (1986) suggests that higher frequency absorption must be relatively lower.

In this respect, we note a second feature of the $J=3-2$ spectrum which is all but absent at $J=2-1$; the strong, and somewhat unexpected emission components at $V_{LSR} \sim 29\,\mathrm{km\,s^{-1}}$. One possibility, of course, is that there is a low velocity, narrow component of optically thin emission in this source. In this respect (and perhaps fortuitously) a similarity to the optically thin profiles of certain outflow sources is notable (cf. Kuiper et al., 1976), although we see no reason why the $J=2-1$ profile is in that case so different. Similarly, it might be argued that the self-absorption is less (and intrinsically narrower) at $J=3-2$, than it is for the lower frequency $J=2-1$ transition. This would have the effect of increasing the overall line intensity, whilst at the same time increasing the value of T_R^* (peak) $- T_R^*$ (dip). It is difficult, for reasons previously considered in Sect. 2, however, to establish a realistic LVG model which would simulate this trend.

As a result, therefore, we are inclined to believe that the disparities in low-velocity line intensities reflects either peculiar emission zone characteristics ($\log X(dv/dr \lesssim -8$, $\log n(H_2) \gtrsim 5$ for $T_K \sim 25$ K) or, and perhaps more reasonably, the effects of beam dilution for a source with $B/D > 1$ (where B is the beam diameter). In this latter respect, we note that a source having $T_B(J=2-1) \simeq T_B(J=3-2)$ might reproduce the approximate variation in peak intensities providing its diameter, D, is of order 45 arcsecs.

Finally, and as in the HCO^+ and CO data of Little et al. (1983) and Matthews et al. (1984), the central spectra display asymmetric and rapidly varying profiles. Whilst the S/N of this data is clearly quite low, we have attempted to roughly delimit the outflow zones in Fig. 26. This confirms that the strongest emission in both wings is located to the north and east of the maser position, and that the respective zones are reasonably closely overlapping. The flow, in short, is far from being that expected of a tilted bipolar source. Furthermore, the present results confirm that the flow is not particularly well collimated, as might be expected given the possible stellar drift, and disk precession noted earlier.

11. NGC 1333 (IRAS 1)

IRAS CPC mapping of the NGC 1333 cloud reveals a complex of far infrared emission, with most of the flux apparently concentrated in ten or so compact sources (Jennings et al., personal communication). Most of these regions appear concentrated in a narrow ridge about RA (1950) = 3^h26^m, and extending from just south of the Herbig Haro cluster HH7-11 discussed in Sect. 9. At least one bright source however appears to be separated from the group, and is located at RA (1950) = $3^h25^m33^s.6$, and DEC (1950) = 31°03′04″; a source we will refer to as IRAS 1 in the proceeding discussion. In the following, we will discuss CO $J=3-2$ and $J=2-1$ results for this region, as well as presenting a 2 cm VLA map of the core.

The CO $J=2-1$ observations cover an area of approximately 3×4 arcmin^2, whilst the $J=3-2$ observations were taken over a more limited region of size 2×3 arcmin^2. Beam sampling was of order ~ 42 seconds in both cases. Mapping of T_R^* (peak) for the

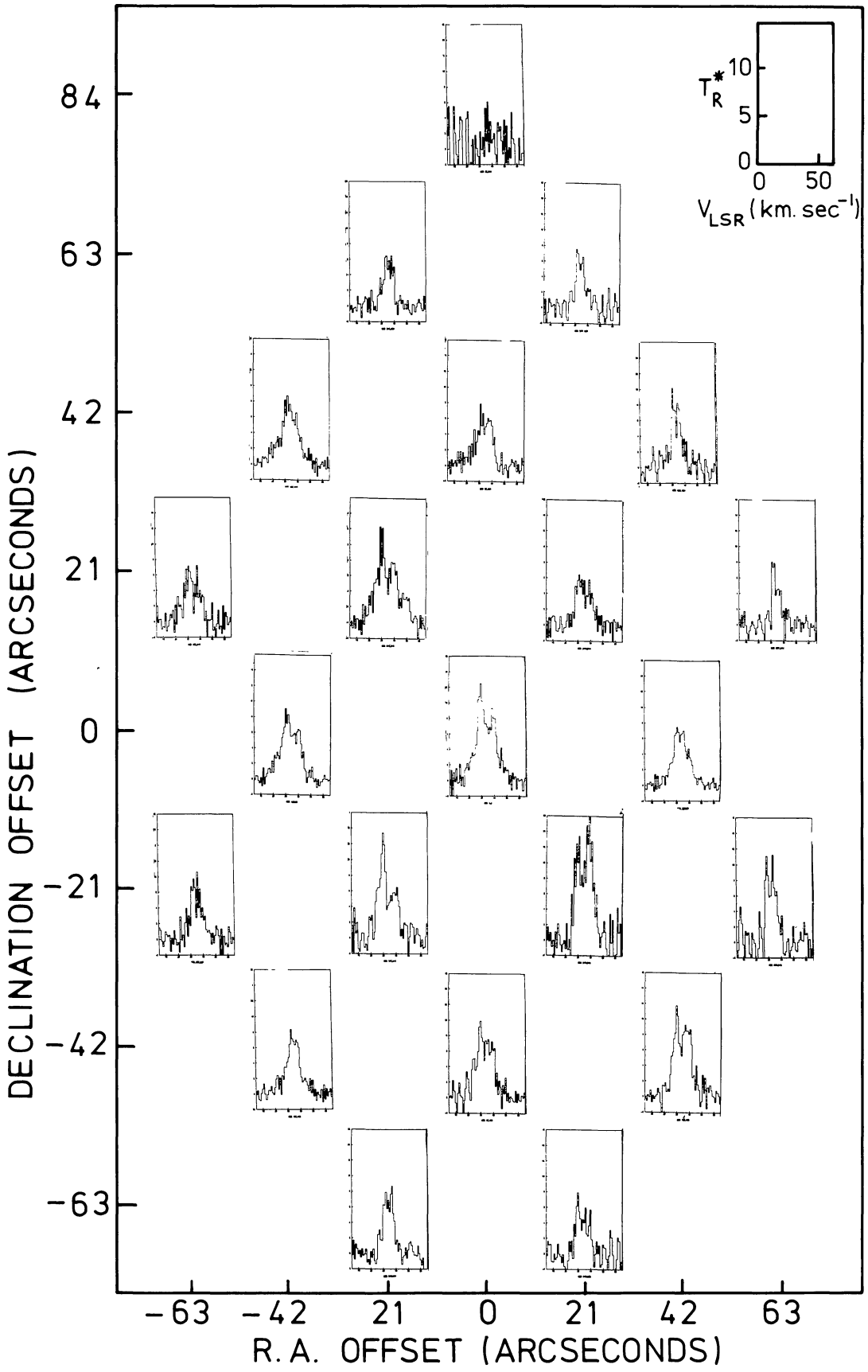

Fig. 24. CO $J=3-2$ spectra of G35.2-0.74. The [0,0] offset position corresponds to the reference location in Table 1

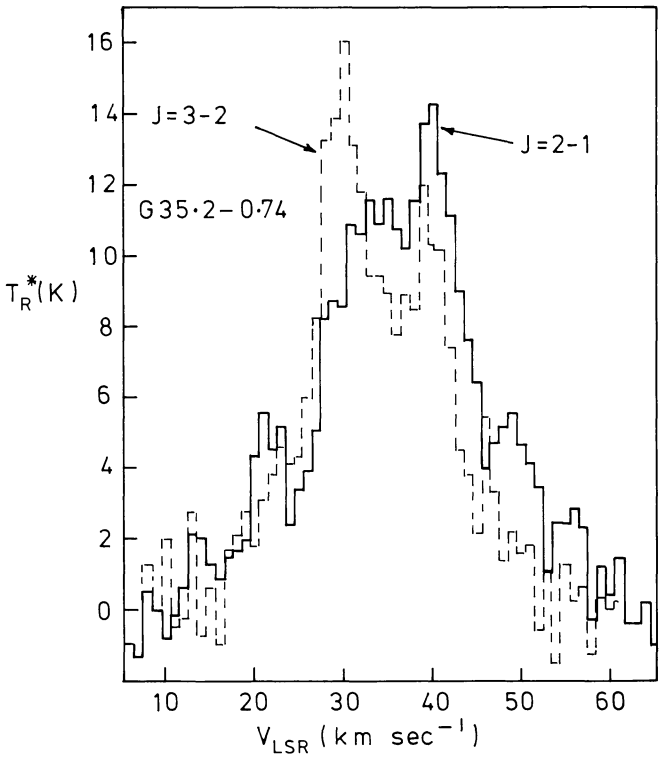

Fig. 25. Comparative CO $J=2-1$ and $J=3-2$ spectra for the [0,0] position in G35.2-0.74

$J=2-1$ transition shows that peak temperatures (~ 14 K) occur to the south-east of the reference position, where the line velocity widths appear also to peak (Fig. 27). Integrated line-wing emission plots are also illustrated in Fig. 27, from which it is apparent that the blue- and red-shifted emission distributions differ quite appreciably; CO $J=2-1$ blue wing emission appearing concentrated to the south and east, whilst red emission components are prominent north-east of the reference position. The source, in short, appears to display the characteristic properties of a bipolar, moderate velocity outflow source. This is further illustrated in Fig. 28, where we show typical spectral profiles from the blue (120E 60S) and red (0E 60N) wing areas of the source; the distinct and varying asymmetries are readily apparent. The less extensive spread of $J=3-2$ spectra show broadly similar characteristics, although the poorer signal to noise (and more limited spectral sampling) precludes a useful comparision of the $J=3-2$ and $J=2-1$ wing emission distributions. Individual $J=3-2$ and $J=2-1$ spectra are, however, directly compared in Fig. 29, and the full complement of $J=3-2$ spectra is illustrated in Fig. 30. It is clear, from this, that individual profiles differ quite radically as between the two transitions, both in respect of line intensity and line shape. In both of these cases, the core ratio $T_R^*(J=3-2)/T_R^*(J=2-1)$ takes a characteristic value of order $\sim 0.8 \rightarrow 0.65$ at low velocities ($V_{LSR} \sim 7$ km s^{-1}) declining to ~ 0.4 at higher velocities ($V_{LSR} \simeq 10$ km s^{-1}). There is also some evidence that the ratios may be larger in the wings ($V_{LSR} \lesssim 6$ km s^{-1} and $V_{LSR} \gtrsim 12$ km s^{-1}), perhaps approaching unity, although the data here is extremely noisy and such conclusions must be regarded with caution. Caution should similarly be expressed in view of the differing beam sizes employed (a factor 1.5 difference in beam diameters) although it is clear from the maps of T_R^* (peak) and integrated wing intensities that, for these regions at least, the emission is reasonably extended at most velocities with respect to the beam. In the main, therefore, T_R may be determined by increasing the values of T_R^* by a factor ~ 1.2. Under these circumstances, peak temperatures $T_R(J=2-1)$ would then approach ~ 10 K, implying excitation temperatures of order ~ 15 K.

If the relatively low intensities are taken to reflect prevailing kinetic temperatures, then it is clear from Fig. 3 that such small ratios for $T_R(J=3-2)/T_R(J=2-1)$ are by no means unexpected – providing that densities $n(H_2)$ are also low. For $T_K \simeq 20$ K, for instance, and taking the typical values $T_R^*(J=2-1)=7.5$ K, $T_R^*(J=3-2)=4$ K, we determine $\log n(H_2) \lesssim 3.75$, and $\log(X/dv/dr) \gtrsim -6$.

Finally, we have acquired a 2 cm VLA map (D configuration) for the position of IRAS 1, taken during August 1984 with the dual IF channel continuum system. The results take the form of a 15 min "snapshot" referenced against a nearby calibrator, which was in turn bootstrapped to 3C 48. As a result, the peak target flux of 3.13 mJy is believed to be accurate to within 20%. As can be seen from Fig. 31, a compact source is located very close to the reference position, and appears barely (if at all) resolved. Assum-

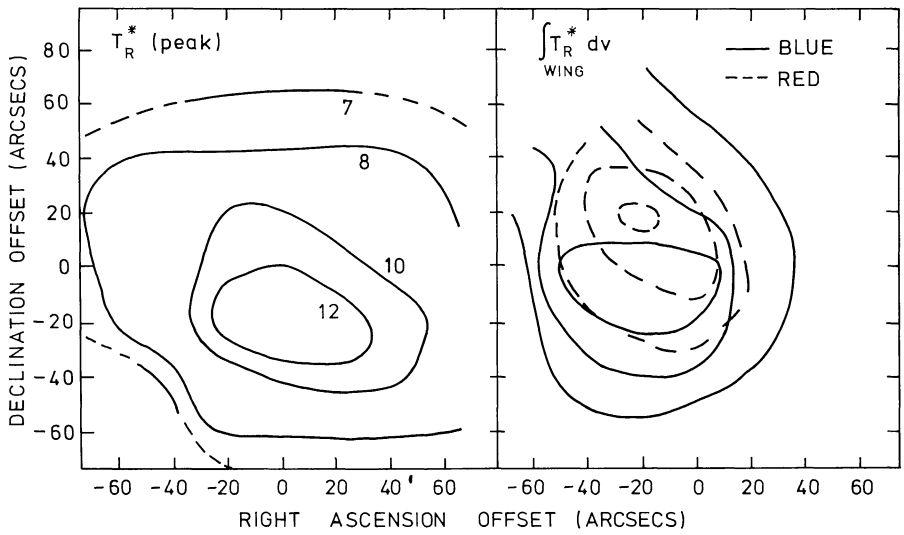

Fig. 26. Variation of peak $J=3-2$ CO antenna temperature T_R^*, and integrated wing emission distributions in G35.2-0.74

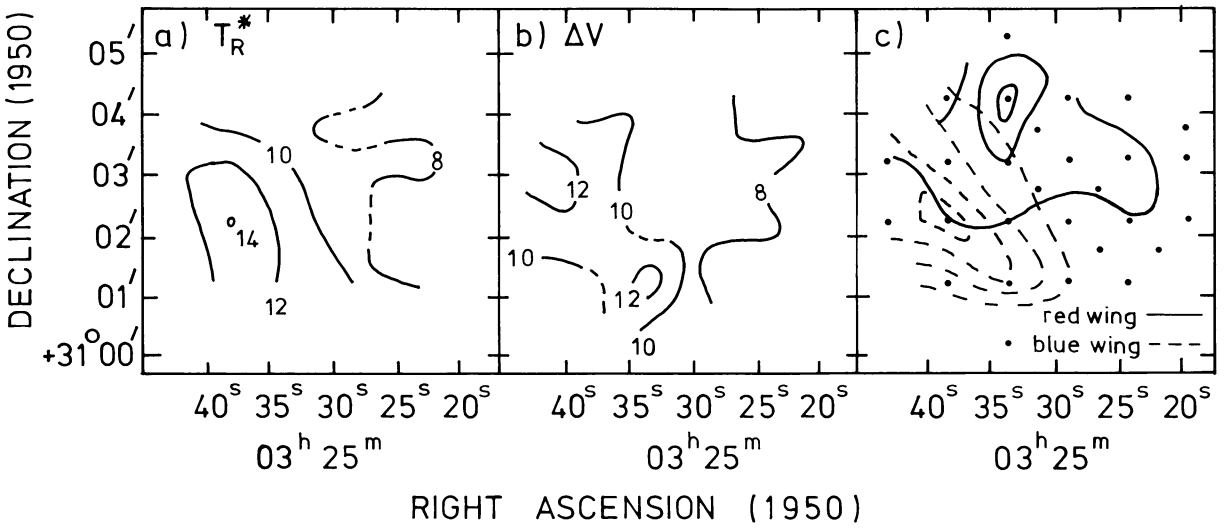

Fig. 27. $J=2-1$ CO variation in line width at the $T_R^* = 1$ K level, peak temperature T_R^*, and integrated red ($-2 \leqq V_{LSR} \leqq 3.5\,\mathrm{km\,s^{-1}}$) wing emission distribution in NGC 1333 (IRAS 1). Contours in panel (c) are set at increments of $2\,\mathrm{K\,km\,s^{-1}}$, with the lowest contours corresponding to $4\,\mathrm{K\,km\,s^{-1}}$

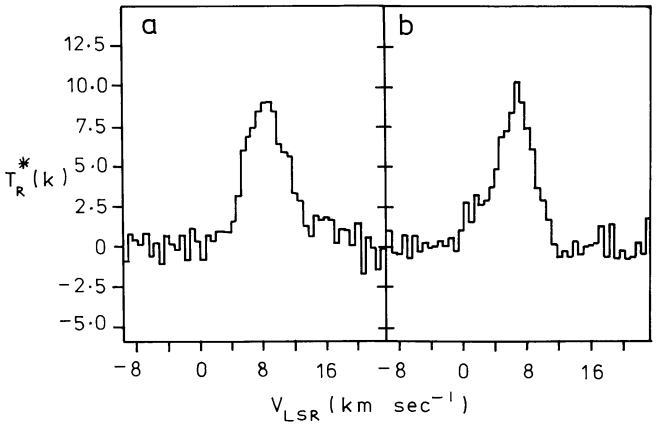

Fig. 28. $J=2-1$ CO spectra from the positions (a) 0 E, 60 N, and (b) 120 E, 60 S of the [0, 0] reference position in NGC 1333 (IRAS 1) (see Table 1)

ing the emission to arise from an optically thin H II region (we have no spectral index data at the present time), then the 2 cm flux is consistent with a Lyman continuum ionising flux of $7.9\ 10^{43}$ photons s^{-1} (taking a distance $D=0.5$ pc similar to that of the nearby HH 7-11 complex). Such a flux would be consistent with radiative ionisation by a single B3 ZAMS star, and this would in turn imply a stellar luminosity $\sim 10^3\,L_\odot$. Infrared photometry however appears to indicate a total flux for IRAS 1 of order $\sim 25\,L_\odot$ (Jennings et al., personal communication), some forty times lower.

It is conceivable, therefore, that either the source ionisation has a large collisional component, or alternatively that the degree of source clumping is large, enabling stellar radiation to escape largely unabsorbed. To explain the observed extinction, this latter hypothesis would require a preferential alignment of absorbing material along the line of sight, provided by such as an accretion disc orientated perpendicularly to the plane of the sky. Given the large discrepancies between the infrared and radio fluxes, however, such an hypothesis would seem at best unlikely. Another question concerns the FIR colour temperature of the source, which from the IRAS data appears to be of order ~ 50 K. The CO mapping data presented here, on the other hand, would appear to indicate an excitation temperature some four times lower, and reveals no evidence for enhanced local temperatures (or "hot spots"). This, in turn, might be explainable if the source is inhomogeneous (leading to beam dilution $W \sim 0.25$), or the thermal coupling between gas and dust is poor.

It is clear from the above, therefore, that this isolated source has various interesting characteristics, and appears to consist of a (low?) luminosity star embedded in a low density cloud. This, in turn, shows evidence of a bipolar flow, driven (perhaps) by a collisionally ionised wind. The number of caveats expressed here, however, is sufficient to indicate that much further work is required, and near-infrared spectroscopy of the core (together with further radio continuum measures) would be of particular interest.

12. Discussion

In the previous sections of this paper we have provided a detailed analysis and discussion of ten high velocity molecular outflow sources. An interesting factor in this analysis has been the inability to model several of these sources in terms of a simple LVG model, or variants thereof; a feature which appears to extend over most of the velocity range for NGC 1333 (HH 7-11). Under these circumstances, it follows that any LVG solution obtained for the line wings must be viewed with at least a modicum of suspicion. There is little doubting that few of the outflow regions reproduce the classical LVG models enumerated by Goldreich Kwan (1974); it is unlikely that jets in such sources will oblige us by maintaining a constant gradient dv/dr. Nevertheless, over limited régimes of the jet outflows dv/dr can undoubtedly be approximated by a unitary value, and emission at any particular V_{LSR} viewed as emission-weighted average of several such regions (providing internal self-absorption does not appreciably modify molecular excitation). It is probable, in short, that such values of $\log(X(\mathrm{CO})/dv/dr)$ and $\log n(\mathrm{H_2})$ as we can derive for these regions are at least broadly indicative of the conditions in the outflow. In the present analysis, we have noted that the relative line strengths

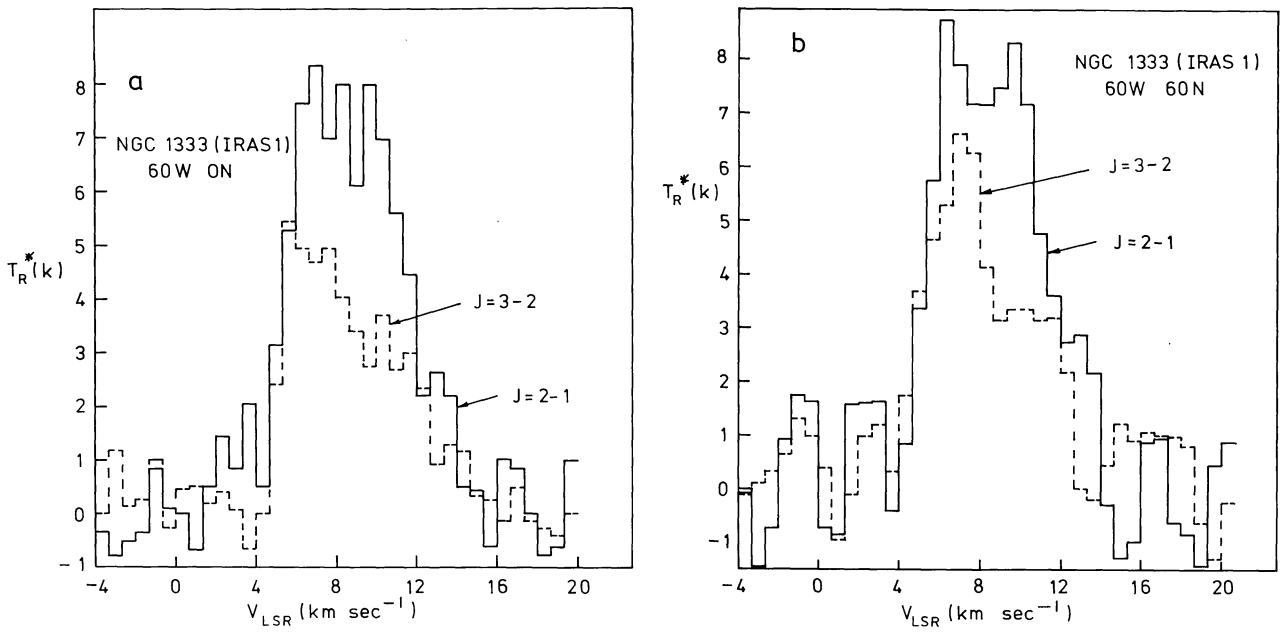

Fig. 29. Comparative $J=2-1$ and $J=3-2$ CO spectra for the positions (a) 60 W, O N and (b) 60 W, 60 N of the [0,0] reference location in NGC 1333 (IRAS 1) (Table 1)

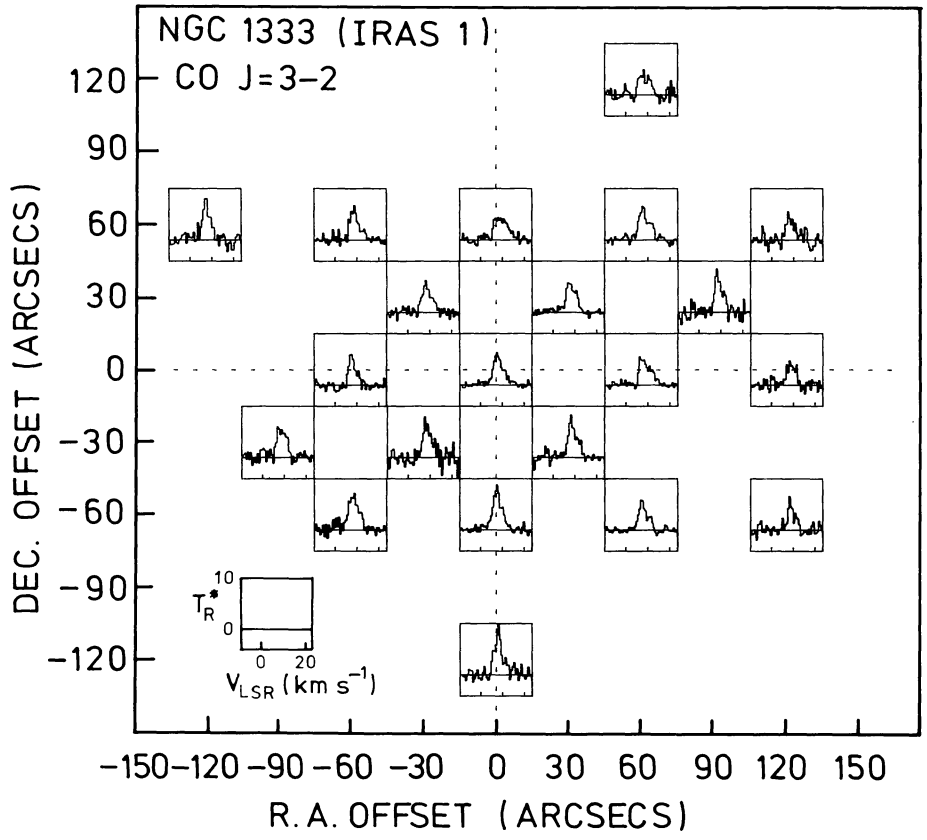

Fig. 30. $J=3-2$ CO spectra of NGC 1333 (IRAS 1). The [0,0] offset position corresponds to the reference location in Table 1

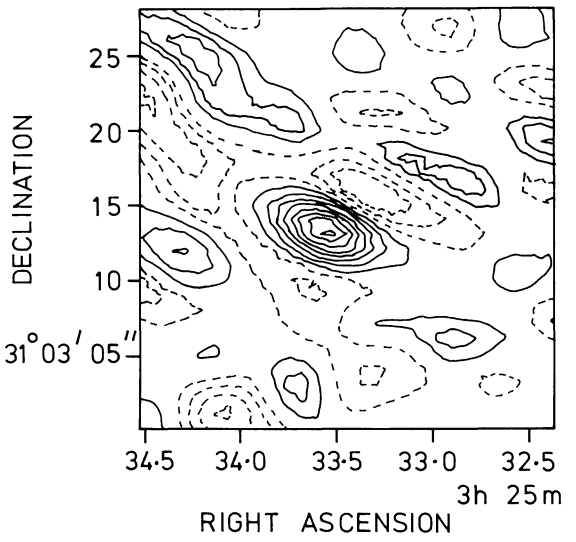

Fig. 31. 2 cm VLA "snapshot" map of the [0,0] position in NGC 1333 (IRAS 1). The contours are in increments of 0.4 mJy with the lowest solid contour corresponding to 0.2 mJy. The central bright source is spatially unresolved

$T_R(J=3-2)/T_R(J=2-1)$ often vary quite appreciably with V_{LSR}, implying a wide range of (velocity dependent) conditions within the outflows themselves. In very few cases is it possible to evaluate these changes over more than a limited range of values V_{LSR} – the S/N of the present $J=3-2$ and $J=2-1$ data is simply not of a high enough standard. Under these circumstances, therefore, other workers (cf. Richardson et al., 1985) have chosen to ratio the integral wing fluxes $\int_{wing} T_R^* dv$.

Such a procedure, in view of the comments expressed earlier, is clearly a policy of desperation; emission from the outflows is frequently weighted at differing values of V_{LSR}, depending upon the transition $J \rightarrow J-1$, and an analysis of mean wing strengths can be regarded as a comparison between differing mean velocities $\bar{V}_{LSR}$. Nevertheless, such procedures are of interest, enable the determination of perhaps more representative excitation conditions for the outflows as a whole, and the evaluation of "mean" temperature ratios having a higher S/N. With this in mind, therefore, we have estimated mean wing temperatures $\bar{T}_{wing}$ for six of our present sources, where

$$\bar{T}_{wing} = \frac{\int_{wing} T_R \, dv}{\Delta V_{wing}}$$

and ΔV_{wing} is the total wing velocity extent; the consequent revised values of $n(H_2)$ and $X(CO)/dv/dr$ are summarised in Table 2. The kinetic temperature was initially assumed to take a value close to the $J=1-0$ excitation temperature (in conformity with the practice in Sect. 2–11), although where this did not result in a viable solution, a more general search of the régime $10 < T_k < 10^2$ K was instituted. The consequence, as may be seen, is that whilst the solutions differ in detail from those discussed earlier (see also Fig. 32), the general trends are qualitatively very similar.

The LVG results at specific velocities V_{LSR} are further illustrated in Fig. 32, whence it is apparent that none of the solutions falls remotely close to the trend expected for stable clouds, or indeed for clouds in free-fall collapse; a régime based upon the analysis outlined in Sect. 5. This disparity is of course hardly surprising, since it is statistically improbable that any of these sources are likely to be collapsing (cf. Field, 1978), and the energetic outflows represent strong evidence against local sta-

Table 2. Mean wing properties for homogeneous ($W=1$) and clumpy ($W=0.33$) outflows

SOURCE	WING	$\bar{T}_{WING}$ (K) J = 1-0	J = 2-1	J = 3-2	W	T_K	Log $n(H_2)$ cm^{-3}	log $X(CO)/dv/dr$ $km^{-1}sec.pc$
NGC 2024	BLUE	4.25	5.08	1.11	1.0	-	*	*
					0.33	-		
	RED	0.76	2.90	2.35	1.0	35	4.1	- 7.6
					0.33	90	4.0	- 7.0
S140	BLUE	3.60	3.72	1.63	1.0	35	3.4	- 6.3
					0.33	35	3.3	- 5.6
	RED	1.73	2.83	2.64	1.0	35	4.0	- 7.1
					0.33	35	4.1	- 6.7
CRL 2591	BLUE	2.0	1.55	1.03	1.0	-	*	*
					0.33	60	2.95	- 5.6
	RED	1.71	1.01	1.77	1.0	-	*	*
					0.33	-	*	*
S88	BLUE	-	4.03	3.03	1.0	40	3.9	- 7.05
					0.33	40	3.9	- 6.6
NGC 1333 (HH7-11)	BLUE	1.96	2.33	2.46	1.0	-	*	*
					0.33	-	*	*
	RED	0.92	4.32	3.21	1.0	40	4.1	- 7.5
					0.33	90	3.9	- 6.5
G35.2 - 0.74	BLUE	-	3.41	3.01	1.0	90	3.8	- 7.0
					0.33	90	3.8	- 6.4
	RED	-	3.50	0.97	1.0	20	< 3.5	> - 6.5
					0.33	-	*	*

* Solutions not available in the régime $10 < T_K < 10^2$ K.

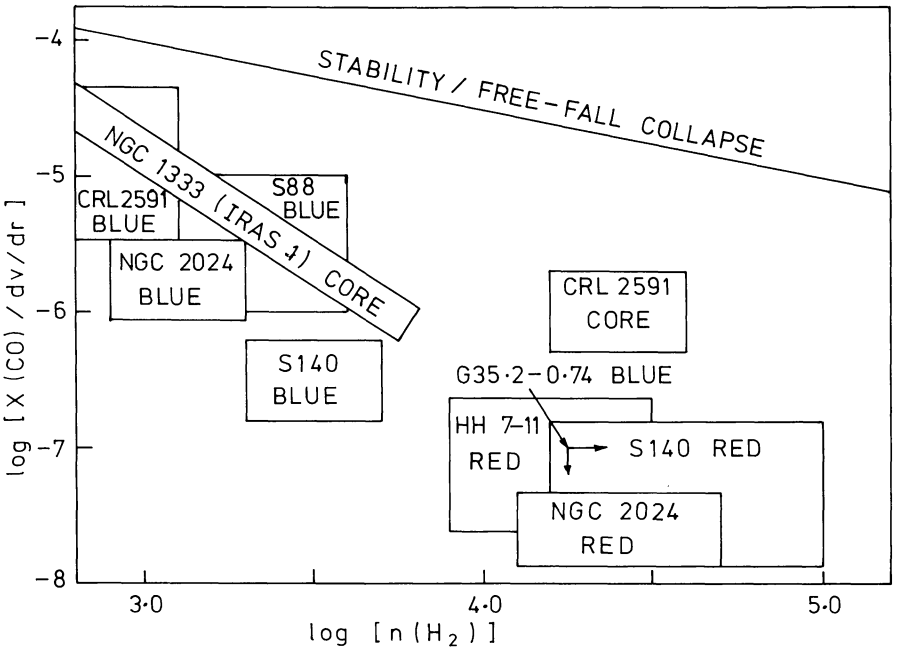

Fig. 32. LVG wing and line core solutions for sources investigated in the present study. The solid line represents the approximate regime for free-fall collapse, or thermal, rotational, and turbulent equilibrium, and the squares indicate the typical sizes of error in $n(H_2)$ and $X(CO)/dv/dr$

bility. It is, nevertheless, of great interest to note that even line core regions have very low values of $\log(X(CO)/dv/dr)$. A second feature of interest is the presence of a distinct trend in solutions within the $\log(X(CO)/dv/dr) - \log(n(H_2))$ plane – a trend one might almost characterise as an outflow "main sequence". Very broadly, this can be represented by a function

$$\frac{dv}{dr} \sim 2.5\ 10^{-4}\, n(H_2)^{3/2} \quad \mathrm{km\,s^{-1}\,pc^{-1}}$$

$(X(CO) = 5\ 10^{-5})$

although it is unclear how such a trend, if real, is related to the evolution of outflow energy, the variation in source kinematic structures, and so forth. Specifically, for instance, one might deduce an evolutionary sequence in which less evolved outflows possessed high densities, large velocity gradients, and therefore small values of $X(CO)/dv/dr$, placing the younger more compact sources to the lower right of Fig. 32. In reality, however, it is apparent that the same source is often represented at both low and high densities. We should also emphasize that the values of V_{LSR} selected for analysis represent differing régimes of the outflows. Perhaps, therefore, the trend in Fig. 32 represents some variation through the flows themselves, a trend which, for $n(H_2) \propto r^{-2}$, say, would imply a plausible velocity law of form $dv/dr \lesssim r^{-3}$; presumably indicative of a phase of rapid initial acceleration. If, on the other hand, a constant rate of mass flow is assumed $(4\pi r^2\, n(H_2)\, V(r) = \text{constant}$, tantamount to assuming an invariant mass loss rate), and more general velocity law of form $V(r) \propto r^{\alpha}$ adopted, then we would obtain the relation $dv/dr \propto n(H_2)^{(1-\alpha)/(2+\alpha)}$; a trend which (equated with the observed variation) would imply a velocity decrement of order $V \propto r^{-4/5}$.

A final point of analysis relates to the structural information buried within this plot. In the case of S88, for instance, the total blue wing velocity extent divided by the width of the outflow indicates a maximum $\Delta V/\Delta R \sim 28\,\mathrm{km\,s^{-1}\,pc^{-1}}$. This, in fact, is not grossly disparate with the value which would be obtained for the blue wing solution in Fig. 32 ($\sim 16\,\mathrm{km\,s^{-1}}$ for $X(CO) \sim 5\ 10^{-5}$). Similarly, the NGC 2024 blue wing would imply $\Delta V/\Delta R \sim 24\,\mathrm{km\,s^{-1}}$, compared to the value $dv/dr \sim 28\,\mathrm{km\,s^{-1}}$ derived from Fig. 32. For these cases at least, therefore, it would seem that the observed physical extent of the wing is consistent with a gradual variation in velocity, and a uniform dv/dr. For the NGC 2024 red wing, however, we determine $dv/dr \sim 2.5\ 10^3\,\mathrm{km\,s^{-1}\,pc^{-1}}$, and for this and other cases to the lower right of Fig. 32, it is clear that the physical extent of the outflow is inconsistent with a uniform variation of velocities throughout the outflow volume.

Richardson et al. (1985), obtaining a qualitatively similar result, suggest that the excessively low values $X(CO)/dv/dr$ may reflect reduced abundances $X(CO)$, rather than enhanced values of dv/dr. There is unfortunately, at present, no clear way of discriminating between these choices; either option is feasible. Further observations at higher resolution would represent a great aid in clarifying this issue. Lower frequency high resolution CO maps are, however, already emerging from facilities such as the Nobeyama 45 m and Kitt Peak 12 m telescopes, and these reveal that much of the emission in bipolars such as L1555 and NGC 2024 (White et al., in preparation) appears to be concentrated at the boundary of the outflow lobes. Similarly, where [as in the case of S140 (see earlier)] the ^{13}CO wing optical depths are low, and deduced local densities are high, it is clear (barring an unusual kinematic structure) that wing emission zone depths must be low. This increasing weight of observational evidence is also supported by certain recent models of bipolar outflow, in which the principal emission is confined to the edges of the outflow cavity, and shock compression and refraction result in relatively small emission zone volumes (cf. Uchida and Shibata, 1984, 1985).

Under these circumstances, therefore, it is clear that values of $\Delta V/\Delta R$ based on the full width ΔR of the outflow region must lead to a gross underestimate of the local velocity gradient. Similarly, it is apparent that such models might also be relevant in understanding the large local densities $n(H_2)$ derived from LVG analyses. In this respect, it is of interest to note that the sizes ΔR of the emission zones derived from equating $\Delta V_{wing}/\Delta R$ with dv/dr (taken from Fig. 32), are commensurate with the dimensions which would arise from the compression of a uniform ambient medium of density

$n(H_2) \sim 10^3\,cm^{-3}$, to form the observed outflow densities $n(H_2) \sim 10^4 \rightarrow 10^5\,cm^{-3}$. The (isothermal) shock velocities required for a compression ratio of ~ 10, however, are relatively modest, and of order $\sim 10\,c_s \sim 10\,km\,s^{-1}$ (where c_s is the local sonic velocity); a value which is significant lower than the typical wing velocity extent ΔV_w.

On present evidence, therefore, we believe that the results in Fig. 32 favour high velocity gradients in at least a proportion of the sources investigated here. It appears, furthermore, that the value of dv/dr is either a strong function of the sampled flow region (as indicated earlier), or varies appreciably between the differing wings; a feature which might reflect variations in ambient density, and the resultant deceleration of the outflow jet. In this context, we note that most of our analysis is based upon results centred on, or close to the central driving source. Under these circumstances, therefore, it is possible that whilst parts of the outflow are undergoing unconfined expansion, others are undergoing severe compressive deceleration related to near-source collimation processes.

None of these conclusions and results are entirely free of caveats, however, and the influence of outflow clumping may for instance be severe [cf. Plambeck et al. (1983); although Cánto (personal communication) finds that published CO and ^{13}CO spectroscopy indicates a low degree of clumping]. The influence of moderately high clumping (leading to a dilution $W = 0.33$) is noted in Table 2, where we have selected values of T_R according to the same criteria as before; errors in $\log X/dv/dr$ and $\log n(H_2)$ are of typical order ± 0.3 dex. The overall consequence seems to be that values of $X(CO)/dv/dr$ are increased by a factor $\approx W^{-1}$, whilst densities are essentially unchanged; a trend which appears to be very approximately replicated down to $W \sim 0.1$. It is conceivable, therefore, that the values of $X(CO)/dv/dr$ in Fig. 32 are somewhat underestimated – although unless W is exceptionally low, $X(CO)/dv/dr$ is likely still to be small, and well displaced from the trend of values expected for stable clouds. Further spectroscopy of CO and ^{13}CO at similar resolutions would be of great aid in helping to define W, and in placing further constraints upon these solutions.

Finally, we note that the large intensity ratios $\Phi_{2/3}$ observed in NGC 1333 (HH 7-11), NGC 2024, and S 140 are unlikely to be explained in terms of a more general velocity law of form $V \propto r^{\alpha}$, say. The local photon escape probability takes a form

$$\beta = \frac{1}{2}\int_{-1}^{+1} \frac{1-e^{-\tau}}{\tau}\, d\mu_m$$

for instance, where $\theta = \cos^{-1}\mu_m$ is the angle between the radius vactor and the line of sight. For a power-low velocity field, therefore, and where (as in the present case) line core optical depths are large, β takes a limiting value $\sim \tau_R/(0.67 + 0.33\alpha)$ (where τ_R is the radial component of optical depth). Under these circumstances, the conditions of local excitation are closely similar to those pertaining in the "standard" LVG model, wherein $V \propto r$; and whilst the effective velocity gradient now takes the form $V/[R(0.67 + 0.33\alpha)]$, the limits upon Φ are expected to be no different from those defined in Fig. 3.

A further contribution to anomolous line ratios has been considered by Carroll and Goldsmith (1981). In this case, infrared continuum pumping of molecules between adjacent vibrational states might result in varying relative transition strengths, and preferential enhancement of the lower frequency transitions. For this to be relevant for the $J = 1-0$ CO transition, however, it is apparent that two criteria need to be met; first, that the radiation field temperature exceeds a value

$$T_s \simeq \frac{h\nu}{K \ln\left(\frac{A_{J+1\rightarrow J}}{A_{V\rightarrow V-1}}\right)} \sim 160\,K,$$

where the A terms correspond to the Einstein spontaneous transition rate for rotational (J) and vibrational (V) transitions. In addition, molecules must reside within a distance r_s of the irradiating source, whence

$$r < r_s \simeq 1.5\ 10^4\, e^{-\frac{1500}{T_s}}\, R_{pc}(T_s) \sim 1.3\, R_{pc}(T_s)\,pc,$$

where $R(T_s)$ is the radius at which local (optically thick) dust radiation temperatures take a value $T_{gr} = T_s$. It is clear, therefore, that for pumping to be relevant the size of the pumping régime cannot greatly exceed the zone wherein $T_{gr} > T_s$, and for a typical source temperature profile (Scoville and Kwan, 1976):

$$T_{gr}(r) = 50\left(\frac{2\ 10^{17}}{r}\right)^{1/3}\ K$$

then $R(T_s)$ takes a value $6\ 10^{15}$ cm, and would subtend an angle of only $\sim 2''.5$ at 1 kpc.

It is apparent, therefore, that the presence of detectable pumping in a CO emission source would require a highly compact (and unresolved) emission core; a feature which is signally absent for the nebulae under consideration here. Whilst many of the sources are clearly quite compact over size scales of 1′, they are in all cases resolved by the present mapping. A further (and related) problem with such a mechanism concerns the observability of these anomalies in the presence of extended CO emission. To illustrate the problem we should note that the mean dust radiation temperature emerging from a radius $R(T_s)$ would be only a little in excess of T_s for an optically thin core (internal, hotter components of dust emission are heavily diluted), and is congruent with T_s where $\tau_d \gg 1$. Given, furthermore, that optically thick CO line temperatures vary as $\sim f W_s T_s$, where the function f takes account of dust/gas thermal coupling (assumed constant), and W_s is the beam dilution corresponding to a source radius R_s, and beamsize B, then the contribution to observed CO brightness temperature would be of order

$$\Delta T_B(CO) \sim 10^3 f \left(\frac{B}{1\,arcmin}\right)^{-2}\left(\frac{D}{1\,kpc}\right)^{-2}\left(\frac{T_s}{50}\right)^{-5} K.$$

It follows, from this, that in a source with temperature varying as $R^{-1/3}$, as assumed here, the value of $\Delta T_B(CO)$ is a strongly varying function of T_s. Furthermore, where T_s is large (corresponding to the inner core emission), then the contribution to observed values of $T_B(CO)$ is low; observed radiation temperatures are primarily reflective of material at distance $r \equiv B$.

It is clear, therefore, that even for enhanced core line temperatures due to pumping, the present sources represent an unsuitable test of the pumping mechanism; line ratios are predominantly determined by the more tenuous, outerlying, and unpumped gas. Furthermore, such effects are also more likely to be detected where $h\nu_{V\rightarrow V+1}/K$ is significantly $\lesssim 3000$ K, as appears to be the case in CS and SiO.

Under these circumstances, and given the additional analysis in Sect. 2, it is apparent that some non-Sobolevian process is most likely to explain the results presented here. This, however, represents an extremely complex problem, wherein local excit-

ation is a function of the overall source thermal, kinematic, and density structure, and the contribution of such factors will be considered elsewhere.

13. Conclusions

We have presented $J=3-2$ and $J=2-1$ CO mapping and spectroscopy for 10 high velocity molecular outflow sources, taken with the CFHT and UKIRT facilities at Mauna Kea. Each source has been discussed in detail and the present data compared (where possible) with previously available $J=2-1$ and $J=1-0$ spectroscopy, enabling a detailed assessment of source structures, kinematics, and densities. Two the sources (S88 and NGC 2264) are shown to be previously unrecognised bipolar outflows, a further recent bipolar discovery is confirmed (NGC 2024), whilst the outflow NGC 1333 (IRAS 1) is investigated here for the first time, and appears also to be strongly bipolar. Appreciable attenuation of $J=3-2$ radiation temperatures (compared to lower frequencies) is found in several cases, and discussed in detail. Such trends are unlikely to reflect varying source structures, and a normal LVG analysis appears incapable of replicating these trends. Similarly, it appears that clumping, self-absorption, infrared pumping, and non-linear velocity fields would be unable to reproduce both the observed line ratios and temperatures. Under these circumstances, it seems possible that a non-LVG solution may have to be invoked, in which either the CO abundance or, say, velocity gradients dv/dr are radially dependent. At least two of the sources show evidence for co-spatial red and blue wings (S140, G35.2-0.74, and also possible K3-50), a situation which may be explicable in terms of bipolar jets having greatly disparate intensities. Under these circumstances, the primary jet would lead to both red *and* blue (co-spatial) wings providing that the outflow collimation was low, and/or the inclination to the line of sight is close to $i\sim\pi/2$. CRL 2591 also appears to represent a source with greatly disparate wing intensities, and this, together with S140, may represent a category of flow in which one of the jets emerges from within the placental cloud, thereby encountering a lower mass of neutral material. Such an hypothesis would also appear consistent with derived LVG parameters; the less confined jet apparently displaying the lower H_2 density $n(H_2)$. A conformity between observed morphology and derived LVG parameters is also to be noted in S88, where again the less confined jet would appear to possess a very much lower outflow density than for the red wing.

Finally, the trend of solutions between wing (or core) densities $n(H_2)$, and the parameter $X(CO)/dv/dr$ suggests a continuous sequence of values having $dv/dr\lesssim n(H_2)^{3/2}$. The values taken by dv/dr are comparable to the ratio $\Delta V/\Delta R$ derived from the mapping ($\sim$wing velocity range/source width) at low densities $n(H_2)$, although at higher values of $n(H_2)$ the implied values of $dv/dr\sim 10^3\,\mathrm{km\,s^{-1}\,pc^{-1}}$ are very much greater (for normal abundances $X(CO)\simeq 5\,10^{-5}$). It is probable, therefore, that strong shock refraction and compression at the edges of the outflow cavity is resulting in both densities $n(H_2)$, and very much narrower primary emission zone widths. Where, as in S140 and NGC 2024, there is also evidence for high and low density components within a single source, then it is possible we are observing a combination of both unconfined expansion, and strong compressive deceleration within the outflow collimation zone. None of the solutions appears consistent with free-fall collapse, or thermal, turbulent, and rotational stability, although $X(CO)/dv/dr$ may be increased if clumping is appreciable.

More specific conclusions relating to the individual sources may be summarised as follows:

1. The bipolar source CRL 2591 was mapped at $J=3-2$ and $J=2-1$, and our results confirm the results of Lada et al. (1984) in implying closely overlapping blue and red wing components. The red components of line velocity are relatively weak at $J=3-2$, and considerably less strong than at $J=2-1$ and $J=1-0$ – a trend that may imply low densities ($n(H_2)\sim$ a few times $10^2\rightarrow 10^3\,\mathrm{cm^{-3}}$) in the redward flow. The blue flow, by contrast, appears to have relatively high densities $n(H_2)$, of order a few times $10^3\rightarrow 10^4\,\mathrm{cm^{-3}}$.

2. W3 was mapped in $J=3-2$, and the spectra show a strong component of self (or at least foreground) absorption, with dip temperatures T_{DIP} $(J=3-2)\sim 8$ K. Such a value compares with peak line temperatures T_{PEAK} $(J=3-2)\sim 22$ K, and lower frequency dip temperatures T_{DIP} $(J=2-1,\ J=1-0)\sim 15$ K.

An analysis of these dip temperatures implies foreground absorption cloud densities of order $\sim 10^3\,\mathrm{cm^{-3}}$, and is consistent with the presumption of Brackmann and Scoville (1980) that the more tenuous, widely distributed CO cloud is responsible for this feature. Our results confirm (or are at least strongly consistent) with the hypothesis that two overlapping clouds are present at the core, with velocities $V_{LSR}\sim -40\,\mathrm{km\,s^{-1}}$ and $V_{LSR}\sim -43\,\mathrm{km\,s^{-1}}$, and separate mapping of the red and blue wing $J=3-2$ line components reveals these clouds to be centred close to IRS 5 and IRS 4 respectively.

3. S88 was mapped at $J=2-1$ and $J=3-2$, and our present results again suggest that the flow is bipolar – albeit the red wings is rather compact. Flow kinetic energies appear to be of order $3\,10^{45}$–$3\,10^{46}$ erg, whilst the outflow momentum is between 48 and $480\,M_\odot\,\mathrm{km\,s^{-1}}$; values which are broadly consistent with what is observed for other HVMOs. Analysis of radial trends in brightness temperature at $J=1-0$, $J=2-1$, and $J=3-2$ suggests that a high density ($n(H_2)\gtrsim 10^4\,\mathrm{cm^{-3}}$) core is located close to, if not coincident with the compact radio source, and may be responsible for a substantial proportion of the foreground extinction. A gradient in central line velocities may also reflect rotation of the central 3 arcmin region of this source, implying corresponding masses $\sim 200\,M_\odot$ where rotational stability is important. For the larger cloud mapped at $J=1-0$, such a result may imply an overall mass $\sim 4\,10^3\,M_\odot$, and mean densities $n(H_2)\sim 1.5\,10^3\,\mathrm{cm^{-3}}$ which are similar to the estimates derived from LVG modelling. There is some evidence for a strong disparity in flow densities, perhaps reflected in the differing spatial extents of the red and blue wing components.

4. NGC 2264 has been mapped at $J=3-2$, from which we find evidence of possible bipolarity. In particular, the blue wing noted by Schwartz et al. (1983) may be optically thin, and enhanced by a factor $\sim 3\rightarrow 7$ over $J=1-0$ when beam dilution is allowed for. Such a bipolar flow would not be consistent with the blister model for this region proposed by Schwartz et al. (1985).

5. K3-50 has been mapped at $J=3-2$, and shows evidence for a rapidly varying FWHM, and a full width at the $T_R^*=1$ K level of $20\,\mathrm{km\,s^{-1}}$. The lines are highly asymmetrical, and show rapid variability in the high velocity components, although there is no clear evidence for bipolarity within the present signal to noise.

6. NGC 2024 was observed at $J=3-2$, and our mapping confirms a bipolarity which has already been investigated by Sanders and Willner (1985) at $J=1-0$. A detailed comparison of the $J=1-0$ and $J=3-2$ maps reveals various disparities, however, with clear evidence for enhanced $J=3-2$ blue wing emission to the east of the outflow source. The exciting source for this region is considered in some detail, as well as the shock

properties of the outflow. It is concluded, in consequence, that local He^+ emission may arise from high shock velocities at the leading edge of the outflow, whilst IRS 2 is responsible for the observed FIR excess, and the associated H II region. The $J=3-2$ radiation temperature is significantly lower than appears to be the case at lower frequencies, and this is discussed at considerable length. The wing densities also appear to be greatly disparate, with model values of order $n(H_2) \sim 10^3\,cm^{-3}$ for the blue wing, and a red wing density in excess of $n(H_2) \sim 10^4\,cm^{-3}$; in consequence of which, red wing values of $T_R(1-0)/T_R(2-1)$ range between ~ 0.2 and 0.5.

7. The source S140 was observed at $J=3-2$, and the profiles at this frequency appear very similar to those at $J=1-0$. A direct comparison of line radiation temperatures, however, reveals the $J=3-2$ line to be very much weaker, a trend which is again difficult to reproduce using LVG models. Wing temperatures were found to be consistent with high densities $\log n(H_2) \sim 3.5 \rightarrow 4.6$. The weak $J=1-0$ red wing is also found to be weak at $J=3-2$, and we discuss the possibility that the source is monopolar, with a flow that is transverse to the line of sight. An alternative explanation in terms of high velocity turbulent elements is also discussed, although it is likely that such an explanation requires high cloud density gradients.

8. The source NGC 1333 (HH7-11) was observed at $J=3-2$, for direct comparison with the $J=2-1$ measurements of Snell and Edwards (1984). As a result, we find that the $J=3-2$ wing emission is enhanced at all of the positions observed by Snell and Edwards (1984), leading to an increase in apparent depth for the self-absorption feature. Attempts to model the $J=1-0$, $J=2-1$ profiles at the source core met with little success, and it is likely that either one (or more) of the profiles is inaccurate, or a simple LVG analysis is inappropriate. An analysis of the $J=2-1$ and $J=3-2$ profiles alone suggests that wing densities may be high, and of order $n(H_2) > 10^4\,cm^{-3}$ (a result also confirmed from analysis of the mean wing temperatures). Here again, however, it proves extremely difficult to model the intensities at the line cores.

9. The G35.2-0.74 region is described in detail, and we provide 22 $J=3-2$ spectra for an area 4.7 arcmin^2 about the northerly maser position, together with a single $J=2-1$ spectrum at the position of the maser. Self-absorption appears, again, to be more prominent at these higher frequencies, and there is also evidence for beam-dilution effects in the relative $J=3-2/J=2-1$ core intensities. A detailed comparison of the central $J=2-1$ and $J=3-2$ profiles reveals that $T_R(J=3-2)/T_R(J=2-1)$ is of order unity for the blue wing, and may take a value >1 for $V_{LSR} > 25\,km\,s^{-1}$. Densities, in consequence, are almost certainly high for both red and blue wings ($n(H_2) \approx 10^4\,cm^{-3}$ or greater). The spatial distribution of $J=3-2$ wing emission reveals that both red and blue components are, in the main, co-spatial, whilst the collimation appears rather poor. It is argued, in consequence, that any outflow is likely to have a low inclination to the line of sight, of order $i \sim \sin^{-1}(\theta/2)$ (where θ is the jet opening angle).

10. Finally, the first observations of an isolated outflow source NGC 1333 (IRAS 1) are discussed. This source was identified through an IRAS mapping procedure, and displays clear ($J=2-1$) evidence for bipolar outflow. This, in turn, appears to be driven by a central source with an apparent FIR luminosity $\sim 25\,L_\odot$; some forty times less than would be derived for the associated compact radio source. The reasons for this disparity are by no means clear, although collisional ionisation may be important, and would lead to an overestimation of the radio luminosity. A large difference is also noted between CO excitation temperatures, and FIR colour temperatures; a result which may imply an inhomogeneous source structure, and/or low thermal coupling between gas and dust. The large ratio $T_R^*(J=3-1)/T_R^*(J=3-2)$ is in this case explicable in terms of low gas kinetic temperatures T_k, and low gas densities $n(H_2)$.

References

Allen, D.A.: 1972, *Astrophys. J.* **172**, L55

Arnal, E.M., Goss, W.M., Dickel, H.R., Forster, J.R.: 1982, *Monthly Notices Roy. Astron. Soc.* **201**, 317

Bally, J., Lada, C.J.: 1983, *Astrophys. J.* **265**, 824

Batchelor, R.A., Caswell, J.L., Goss, W.M., Haynes, R.F., Knowles, S.H., Wellington, K.J.: 1980, *Australian J. Phys.* **33**, 139

Black, J.H., Willner, S.P.: 1984. *Astrophys. J.* **279**, 673

Blair, G.N., Evans, N.J., Vanden Bout, P.A., Peters, W.L.: 1978, *Astrophys. J.* **219**, 896

Blitz, L., Fich, M., Stark, A.A.: 1982, *Astrophys. J. Suppl.* **49**, 183

Brackmann, E., Scoville, N.: 1980, *Astrophys. J.* **242**, 112

Brown, A.T., Little, L.T., Macdonald, G.H., Matheson, D.N.: 1982, *Monthly Notices Roy. Astron. Soc.* **201**, 121

Cesarsky, D.A.: 1977, *Astron. Astrophys.* **54**, 765

Claussen, M.J., Berge, G.L., Heiligman, G.M., Leighton, R.B., Lo, K.H., Masson, C.R., Moffet, A.T., Phillips, T.G., Sargent, I.A., Scott, S.L., Wannier, P.G., Woody, D.P.: 1984, *Astrophys. J.* **285**, L79

Crutcher, R.M., Hartkopf, W.I., Giguere, P.T.: 1978, *Astrophys. J.* **226**, 839

Dent, W.R.F., Little, L.T., Sato, S., Ohishi, M., Yamashita, T.: 1985a, *Monthly Notices Roy. Astron. Soc.* **217**, 217

Dent, W.R.F., Little, L.T., Kaifu, N., Ohishi, M., Suzuki, S.: 1985, *Astron. Astrophys.* **146**, 375

Dent, W.R.F., Little, L.T., White, G.J.: 1984, *Monthly Notices Roy. Astron. Soc.* **210**, 173

Dickel, H.R., Dickel, J.R., Werner, M.W.: 1980, *Astrophys. J.* **237**, 711

Draine, B.T.: 1983, *Astrophys. J.* **270**, 519

Evans, N.J., Blair, G.N., Harvey, P., Israel, F., Peters, W.L., Schottes, M., de Graauw, T., Vanden Bout, P.: 1981, *Astrophys. J.* **250**, 200

Felli, M., Harten, R.J.: 1981, *Astron. Astrophys.* **100**, 42

Field, G.C.: 1978, Protostars and Planets, ed. T. Gehrels, University of Arizona Press, Tucson, Arizona

Forster, J.R., Goss, W.M., Dickel, H.R.: 1982

Franco, J., Cox, D.P.: 1983, *Astrophys. J.* **273**, 243

Frey, Lemke, D., Thum, D., Fahrbach, U.: 1979, *Astron. Astrophys.* **74**, 133

Genzel, R., Downes, D.: 1977, *Astron. Astrophys. Suppl.* **30**, 145

Genzel, R., Downes, D.: 1979, *Astron. Astrophys.* **61**, 117

Goldreich, P., Kwan, J.: 1974, *Astrophys. J.* **189**, 441

Green, S., Chapman, S.: 1978, *Astrophys. J. Suppl.* **37**, 169

Green, S., Thaddeus, P.: 1976, *Astrophys. J.* **205**, 766

Harvey, P.M., Campbell, M.F., Hoffmann, W.F.: 1978, *Astrophys. J.* **215**, 151

Harvey, P.M., Campbell, M.F., Hoffmann, W.F.: 1978, *Astrophys. J.* **219**, 891

Haschick, A.D., Moran, J.M., Rodriguez, L.F., Burke, B.F., Greenfield, P., Garcia-Barretto, J.A.: 1981, *Astrophys. J.* **237**, 26

Hayashi, M., Omadaka, T., Hasegawa, T., Suzuki, S.: 1985, *Astrophys. J.* **288**, 170

Herbig, G.H.: 1974, *Lick., Obs. Bull.* No. 658

Ho, P.T.P., Barrett, A.H.: 1980, *Astrophys. J.* **237**, 38
Icke, V., Gatley, I., Israel, F.P.: 1980, *Astrophys. J.* **236**, 808
Jaffe, D.T., Hildeband, R.H., Keene, J., Whitcombe, S.E.: 1983, *Astrophys. J.* **273**, L89
Jaffe, D.T., Wilson, T.L.: 1981, *Astrophys. J.* **246**, 113
Konigl, A.: 1982, *Astrophys. J.* **261**, 115
Krügel, E., Thorn, C., Martin-Pintado, J., Pankonin, V.: 1982, *Astron. Astrophys. Suppl.* **48**, 345
Lada, C.: 1984 in *Galactic and Extragalactic Infrared Spectroscopy*, eds. M.F. Kessler, J.P. Phillips, Reidel, Dordrecht
Lada, C.J., Elmegreen, B.G., Cong, H., Thaddeus, P.: 1978, *Astrophys. J.* **226**, L39
Lada, C.J., Gautier, T.N.: 1982, *Astrophys. J.* **261**, 161
Lada, C.J., Gottleib, C.A., Litvak, M.M., Lilley, A.E.: 1974, *Astrophys. J.* **194**, 609
Lada, C.J., Thronson, H.A., Smith, H.A., Schwartz, P.R., Glaccum, W.: 1984, *Astrophys. J.* **286**, 302
Little, L.T., Brown, A.T., Riley, P.W., Matthews, N., Macdonald, G.H., Vizard, D.R., Cohen, R.J.: 1983, *Monthly Notices Roy. Astron. Soc.* **203**, 409
Little, L.T., Dent, W.R.F., Heaton, B., Davies, S.R., White, G.J.: 1985, *Monthly Notices Roy. Astron. Soc.* **217**, 227
Loren, R.B.: 1976, *Astrophys. J.* **209**, 466
Loren, R.B.: 1981, *Astrophys. J.* **249**, 550
Loren, R.B., Plambeck, R.L., Davis, J.H., Snell, R.L.: 1981, *Astrophys. J.* **245**, 495
Lortet-Zuckerman, M.C.: 1974, *Astron. Astrophys.* **30**, 67
Margulis, M., Lada, M.: 1985, *Astrophys. J.* **299**, 925
Matthews, N., Little, L.T., Nyman, L.-A., Macdonald, G.H.: 1984, *Astron. Astrophys.* **136**, 282
Norman, C.A., Silk, J.: 1979, *Astrophys. J.* **228**, 197
Perek, L., Kohoutek: 1967, Catalogue of Galactic Planetary Nebulae, Acadamea Publ. House, Czech.
Phillips, T.G., Huggins, P.J., Wannier, P.G., Scoville, N.Z.: 1979, *Astrophys. J.* **231**, 720
Plambeck, R.L., Snell, R.L., Loren, B.: 1983, *Astrophys. J.* **266**, 321
Pudritz, R.E., Norman, C.A.: 1983, *Astrophys. J.* **274**, 677
Richardson, K.J., White, G.J., Avery, L.W., Lesurf, J.C.G., Harten, R.H.: 1985, *Astrophys. J.* **290**, 637
Rodriguez, L.F., Chaisson, E.J.: 1978, *Astrophys. J.* **221**, 816
Sanders, D.B., Willner, S.P.: 1985, *Astrophys. J.* **293**, L39
Sandqvist, Aa., Wootten, A., Loren, R.B., Friberg, P., Hjalmarson, A.: 1982, in *Regions of Recent Star Formation*, eds. R.S. Roger, P.E. Dewdney, Reidel, Dordrecht
Sandqvist, Aa., Wootten, A., Loren, R.B., Friberg, P., Hjalmarson, A., in The Scientific Importance of Submillimetre Observations, ESASP-189
Sargent, A.I.: 1979, *Astrophys. J.* **233**, 163
Schwartz, P.R., Thronson, H.A., Odenwald, S.F., Glaccum, W., Lowenstein, R.F., Wolf, G.: 1985, *Astrophys. J.* **292**, 231
Shull, J.M., McKee, C.F.: 1979, *Astrophys. J.* **227**, 131
Simon, M., Righini-Cohen, G., Felli, M., Fischer, J.: 1981, *Astrophys. J.* **245**, 552
Snell, R.L., Edwards, S.: 1981, *Astrophys. J.* **251**, 103
Snell, R.L., Mundy, L.G., Goldsmith, P.F., Evans, N.J., Erickson, N.R.: 1984, *Astrophys. J.* **276**, 625
Snell, R.L., Loren, R.B.: 1977, *Astrophys. J.* **211**, 122
Solomon, P.M., Huguenin, G.R., Scoville, N.Z.: 1981, *Astrophys. J.* **245**, L19
Strom, S.E., Grasdalen, G.L., Strom, K.M.: 1974, *Astrophys. J.* **191**, 111
Strom, S.E., Vrba, F.J., Strom, K.M.: 1976, *Astron. J.* **81**, 314
Thompson, R.I., Tokunaga, A.T.: 1978, *Astrophys. J.* **226**, 119
Torrelles, J.M., Rodriguez, L.F., Canto, J., Marcaide, J. and Gyulbudaghian, A.L.: 1983, *Rev. Mex. Astron. Astrof.* **8**, 147
Thronson, H.A., Harper, D.A.: 1979, *Astrophys. J.* **230**, 133
Thronson, H.A., Lada, C.J., Schwartz, P.R., Smith, H.A., Smith, J., Glaccum, W., Harper, D.A., Loewenstein, R.F.: 1984, *Astrophys. J.* **200**, 154
Thronson, H.A., Lada, C.J., Hewagama, T.: 1985, *Astrophys. J.* **297**, 662
Turner, B.F., Matthews, H.E.: 1984, *Astrophys. J.* **277**, 164
Uchida, Y., Shibara, K.: 1984, *Publ. Astron. Soc. Japan* **36**, 105
Uchida, Y., Shibata, K.: 1985, *Publ. Astron. Soc. Japan* **37**, 515
Wendker, H.J., Baars, J.W.M.: 1974, *Astron. Astrophys.* **33**, 157
White, G.J., Liitle, L.T.: 1975, *Astrophys. Letters* **16**, 151
White, G.J., Phillips, J.P., Richardson, K., Harten, R.: 1986, *Astron. Astrophys.* **159**, 309
White, G.J., Phillips, J.P., Watt, G.D.: 1981, *Monthly Notices Roy. Astron. Soc.* **197**, 745
Wright, M.C.H., Dickel, H.R., Ho, P.T.P.: 1984, *Astrophys. J.* **281**, L71
Wynn-Williams, C.G., Becklin, E.E., Neugebauer, G.: 1972, *Monthly Notices Roy. Astron. Soc.* **160**, 1
Wynn-Williams, C.G., Becklin, E.E., Matthews, K., Neugebauer, G., Werner, M.W.: 1977, *Monthly Notices Roy. Astron. Soc.* **179**, 255